Neuron

Ventral pallidum DRD3 potentiates a pallido-habenular circuit driving accumbal dopamine release and cocaine seeking

Highlights

- DRD3-mediated plasticity in the VP drives post-abstinence cocaine-seeking behavior

- VP DRD3 signaling regulates dopamine release in the NAc latSh during seeking

- VP DRD3$^+$ projections to the LHb and VTA display differing activity during seeking

- DRD3 signaling/activity of LHb-projecting VP DRD3$^+$ neurons drives seeking behavior

Authors

Horia Pribiag, Sora Shin,
Eric Hou-Jen Wang, ...,
Varoth Lilascharoen, Yulong Li,
Byung Kook Lim

Correspondence

bklim@ucsd.edu

In brief

Pribiag et al. show that ventral pallidum dopamine receptor D3 signaling regulates drug seeking following prolonged abstinence from cocaine self-administration via activation of a subpopulation of neurons projecting to the lateral habenula. This regulation feeds back to influence dopamine release in the lateral shell of the nucleus accumbens during drug seeking.

CellPress

Neuron

CellPress
OPEN ACCESS

Article

Ventral pallidum DRD3 potentiates a pallido-habenular circuit driving accumbal dopamine release and cocaine seeking

Horia Pribiag,[1] Sora Shin,[1,2,3] Eric Hou-Jen Wang,[1,4] Fangmiao Sun,[5,6] Paul Datta,[1] Alexander Okamoto,[1] Hayden Guss,[1] Akanksha Jain,[1] Xiao-Yun Wang,[1] Bruna De Freitas,[1] Patrick Honma,[1] Stefan Pate,[1] Varoth Lilascharoen,[1,7] Yulong Li,[5,6] and Byung Kook Lim[1,4,7,8,*]

[1]Neurobiology Section, Division of Biological Sciences, University of California, San Diego, La Jolla, CA 92093, USA
[2]Center for Neurobiology Research, Fralin Biomedical Research Institute at Virginia Tech Carilion, Virginia Tech, Roanoke, VA 24016, USA
[3]Department of Human Nutrition, Foods, and Exercise, Virginia Tech, Blacksburg, VA 24061, USA
[4]Biomedical Sciences Graduate Program, University of California, San Diego, La Jolla, CA 92093, USA
[5]State Key Laboratory of Membrane Biology, Peking University School of Life Sciences, 100871 10 Beijing, China
[6]PKU-IDG/McGovern Institute for Brain Research, 100871 Beijing, China
[7]Biological Sciences Graduate Program, University of California, San Diego, La Jolla, CA 92093, USA
[8]Lead contact
*Correspondence: bklim@ucsd.edu
https://doi.org/10.1016/j.neuron.2021.05.002

SUMMARY

Drugs of abuse induce persistent remodeling of reward circuit function, a process thought to underlie the emergence of drug craving and relapse to drug use. However, how circuit-specific, drug-induced molecular and cellular plasticity can have distributed effects on the mesolimbic dopamine reward system to facilitate relapse to drug use is not fully elucidated. Here, we demonstrate that dopamine receptor D3 (DRD3)-dependent plasticity in the ventral pallidum (VP) drives potentiation of dopamine release in the nucleus accumbens during relapse to cocaine seeking after abstinence. We show that two distinct VP DRD3$^+$ neuronal populations projecting to either the lateral habenula (LHb) or the ventral tegmental area (VTA) display different patterns of activity during drug seeking following abstinence from cocaine self-administration and that selective suppression of elevated activity or DRD3 signaling in the LHb-projecting population reduces drug seeking. Together, our results uncover how circuit-specific DRD3-mediated plasticity contributes to the process of drug relapse.

INTRODUCTION

Drug addiction is a chronic, often lifelong disorder characterized by high rates of relapse to drug use despite successful abstinence periods (Dong et al., 2017). Through repeated potentiation of the mesolimbic dopamine (DA) system, addictive drugs produce potent and long-lasting changes in gene expression, synapse function, and overall dynamics of neural circuits that control motivated behaviors (Lüscher and Malenka, 2011; Nestler and Lüscher, 2019; Volkow and Boyle, 2018). How this remodeling process is coordinated across different subcircuits of the brain's reward system to mediate relapse to drug use is not well understood.

As an anatomical hub of the ventral basal ganglia circuitry, the ventral pallidum (VP) encodes reward-related information (Ahrens et al., 2016; Fujimoto et al., 2019; Ottenheimer et al., 2020; Richard et al., 2016; Root et al., 2015; Smith et al., 2009; Tachibana and Hikosaka, 2012) and participates in the development of addictive behaviors in response to cocaine and other drugs of abuse (Creed et al., 2016; Farrell et al., 2019; Heins-

broek et al., 2020; Mahler et al., 2014; Pardo-Garcia et al., 2019; Root et al., 2015). VP neurons display altered firing patterns in response to self-administered cocaine (Root et al., 2012) and exhibit synaptic adaptations following repeated cocaine exposure (Creed et al., 2016; Heinsbroek et al., 2017; Kupchik et al., 2014). Reducing the activity of VP neurons during relapse sessions reduces drug seeking in animals previously trained to self-administer cocaine or other drugs of abuse (Farrell et al., 2019; Mahler et al., 2014; McFarland and Kalivas, 2001; Prasad and McNally, 2016; Prasad et al., 2020; Root et al., 2015), underlining a critical role for the VP in mediating drug relapse behaviors. However, how molecular factors mediate drug-induced plasticity in the VP to differentially influence downstream structures participating in relapse to drug use is not known. In addition, while extracellular DA levels are known to rise in the VP during cocaine self-administration (Sizemore et al., 2000), the role of VP DA signaling in mediating the development of drug relapse behavior remains unexplored.

DA receptor signaling is critical to driving synaptic plasticity and drug-seeking behavior that occurs following exposure to drugs of

abuse (Baik, 2013; Bossert et al., 2013; Crombag et al., 2002; Lüscher and Malenka, 2011). In particular, DA receptor D3 (DRD3) antagonism has shown promise as a feasible therapeutic strategy for addiction treatment (Chen et al., 2014; Galaj et al., 2018; Song et al., 2014; You et al., 2019). Compared to D1 (DRD1) and D2 (DRD2) DA receptors, DRD3 has a higher affinity for DA (Richtand, 2006; Robinson et al., 1994; Sokoloff et al., 1990), suggesting that it may serve as a readout of tonic DA levels and/or play a prominent role in regions that receive sparse dopaminergic (DAergic) innervation. DRD3 is preferentially expressed in areas of the brain involved in motivation, reward, and emotion, including the VP, ventral striatum, and lateral septum (Gurevich and Joyce, 1999; Shin et al., 2018; Sokoloff and Le Foll, 2017; Stanwood et al., 2000). DRD3 expression is elevated in several brain areas in response to psychostimulant drugs such as cocaine and amphetamine, both in animal models of addiction (Bahi et al., 2005; Le Foll et al., 2005; Neisewander et al., 2004) and in human addicts (Boileau et al., 2012; Payer et al., 2014; Staley and Mash, 1996). However, the specific contribution of DRD3 signaling to drug-mediated plasticity within neural circuits that drive motivated behaviors remains unknown. Elucidating a circuit-specific role for DRD3 may help unlock the therapeutic potential of DRD3 antagonism as applied to drug abuse.

Here, we undertook a multifaceted approach to understand how DRD3 signaling, neuronal projection-specific activity, and DA release are coordinated by the VP to drive relapse to cocaine seeking. Using a drug relapse assay consisting of cocaine self-administration followed by a 2-week period of forced abstinence and a drug-seeking test, we found that DRD3 signaling in the mouse VP drives relapse to cocaine seeking via context-dependent augmented activity of VP DRD3^{+} neurons. Knockdown (KD) of DRD3 expression in the VP reduces activity of the lateral ventral tegmental area (latVTA) and DA release in the lateral shell of the nucleus accumbens (NAc latSh) during relapse to cocaine seeking, suggesting that the change in activity of VP DRD3^{+} neurons controls drug relapse by influencing the DAergic output of the VTA. Detailed circuit analyses of VP DRD3^{+} neuronal projections to the lateral habenula (LHb) and the VTA revealed that while both projections are capable of elevating NAc latSh DA release when optogenetically stimulated, only LHb-projecting VP DRD3^{+} neurons display tonically elevated activity during relapse to cocaine seeking. Moreover, inhibiting the VP DRD3^{+} projection to the LHb, either optogenetically or chemogenetically, or reducing DRD3 signaling in the VP to LHb projection, suppressed cocaine-seeking behavior following prolonged abstinence, whereas analogous manipulations of the VP DRD3^{+} projection to the VTA did not suppress cocaine seeking. Our results provide a circuit-level understanding of VP DRD3 signaling in driving relapse to drug use and, more specifically, how activity of a molecularly defined output of the VP to the LHb can serve as an effective target in the treatment of drug relapse.

RESULTS

Abstinence from cocaine exposure upregulates *DRD3* expression in the VP

The VP expresses DRD1, DRD2, and DRD3 (Beckstead et al., 1988; Contreras et al., 1987; Mansour et al., 1990; Richfield et al., 1989; Tziortzi et al., 2011) and receives DAergic innervation from the VTA (Del-Fava et al., 2007; Klitenick et al., 1992; Taylor et al., 2014). To assess the impact of cocaine exposure on DA receptor signaling in the VP, we measured *DRD1*, *DRD2*, and *DRD3* mRNA levels using qPCR following passive or self-administered cocaine exposure. Mice injected with cocaine for 5 days (15 mg/kg/day, intraperitoneally [I.P.]) showed a significant elevation of *DRD3* mRNA in the VP, but only after a drug-free period of 10 days (Figures 1A and S1A). Similarly, mice that self-administered cocaine for 10 days showed a significant elevation of *DRD3* mRNA in the VP after 2 weeks of home-cage abstinence (Figure 1B) and a slight trend toward increased expression following 1 day of abstinence (Figure S1B). Thus, we hypothesized that VP DRD3 may participate in the remodeling of gene expression and circuit function that occurs during prolonged withdrawal from cocaine exposure (Dong et al., 2017; Lüscher and Malenka, 2011; Massart et al., 2015; Walker et al., 2018) and that VP DRD3 signaling may be functionally involved in driving relapse to cocaine seeking after prolonged abstinence.

VP DRD3 signaling mediates relapse to cocaine seeking

To understand the role of VP DRD3 signaling in the development of cocaine-seeking behavior, we used adeno-associated virus (AAV)-mediated delivery of small hairpin RNA (shRNA) to robustly knock down *DRD3* expression in the VP, without affecting *DRD1* or *DRD2* expression (Figure 1C). We applied this manipulation, along with a rescue construct co-expressing DRD3 shRNA and a KD-resistant DRD3 mutant (DRD3 Rescue) (Shin et al., 2018), to mice that went on to self-administer cocaine for 11 days, followed by 2 weeks of home-cage abstinence and a seeking test performed under extinction conditions on day 25 (Figures 1D–1F). DRD3 KD in the VP did not alter nose-poke rates under fixed ratio 1 (FR1), FR3, or progressive ratio (PR) schedules in either male or female mice (Figures 1G, S1F, and S1H). In contrast, following 2 weeks of abstinence, the number of drug-seeking nose pokes performed on the side previously paired with cocaine delivery (i.e., active nose pokes) was markedly reduced in both male and female mice expressing DRD3 shRNA in the VP (Figures 1H, S1G, and S1I). Conversely, rescue of DRD3 expression fully restored drug-seeking behavior without affecting consummatory behavior (Figures 1G, 1H, and S1F–S1I). Analogous results were obtained using cocaine-induced conditioned place preference (CPP), with mice expressing DRD3 shRNA in the VP showing significantly reduced place preference after a 10 day drug-free period (Figures S1C–S1E). However, VP DRD3 KD mice did not display significantly altered weight, locomotor activity, or open field anxiety (Figures S1J and S1K). Moreover, VP DRD3 KD mice did not show differences in the consummatory or seeking phases of a sugar pellet self-administration paradigm that mimicked our cocaine self-administration paradigm (Figures S1L–S1N), indicating that the ability to recall an operant task and the motivation to seek a palatable reward remained intact. Taken together, these results support the notion that DRD3 signaling in the VP is a critical and specific mediator of relapse to cocaine seeking following prolonged abstinence.

The VP contains a heterogeneous mix of cell types defined by neurotransmitter identity and other molecular markers (Root
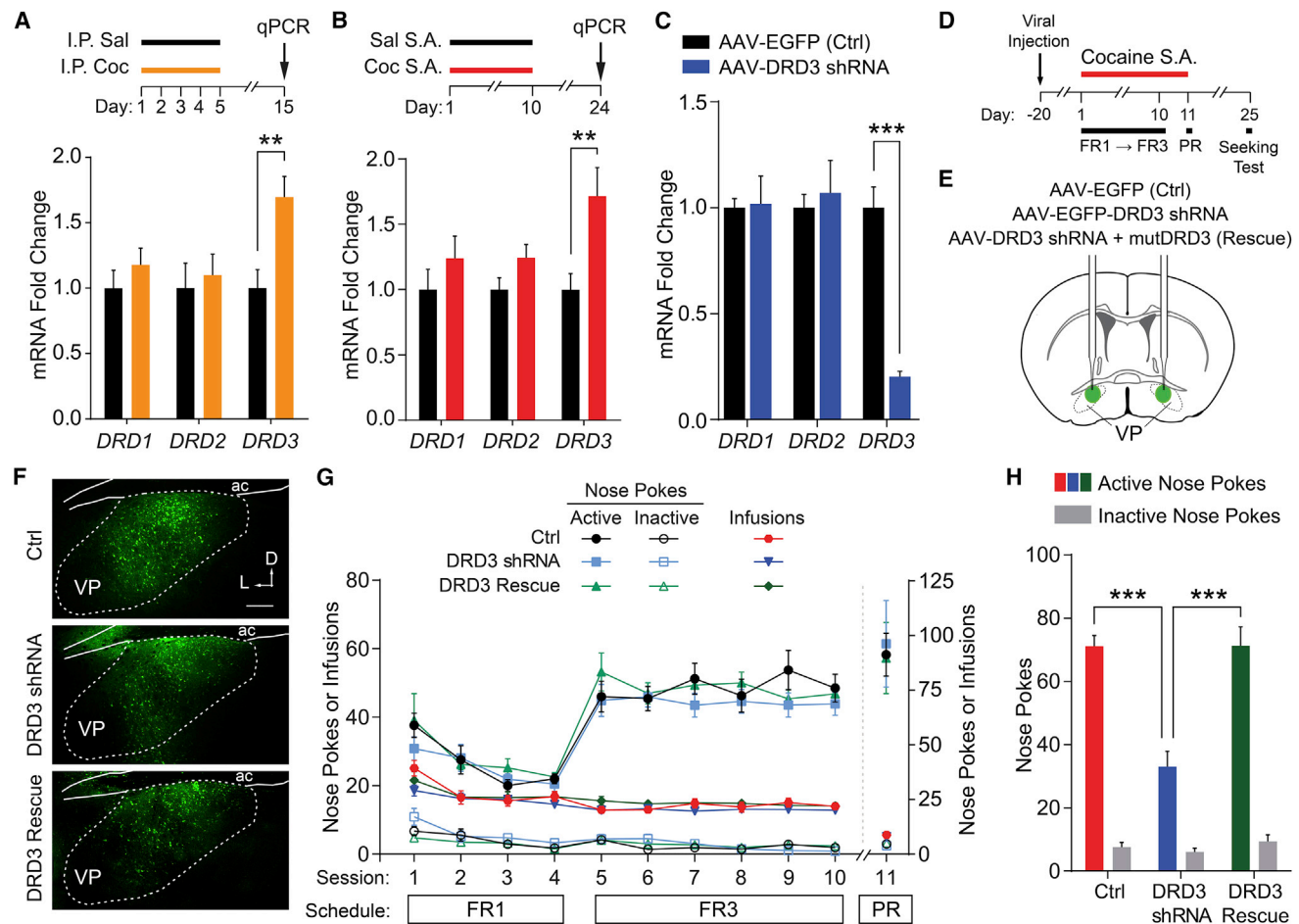
Neuron
Article

CellPress
OPEN ACCESS

Figure 1. VP DRD3 drives relapse to cocaine seeking

(A and B) Noncontingent (I.P.) (A) or self-administered (S.A.) (B) cocaine selectively elevated *DRD3* expression in the VP following prolonged abstinence. For (A), two-way repeated-measures (RM) ANOVA, Sidak's post hoc test, **$p < 0.01$; n = 11, 12 mice for Sal, Coc. For (B), two-way RM ANOVA, Sidak's post hoc test, **$p < 0.01$; n = 9,12 mice for Sal, Coc. Sal, saline; Coc, cocaine.

(C) Selective and robust KD of *DRD3* expression in the VP by AAV-mediated delivery of *DRD3*-targeting shRNA. Two-way RM ANOVA, Sidak's post hoc test, ***$p < 0.001$; n = 6 mice each for control (Ctrl) and DRD3 shRNA.

(D) Experimental schedule of cocaine self-administered experiments.

(E and F) Schematic of bilateral stereotaxic injection of Ctrl, DRD3 shRNA, and DRD3 rescue AAVs into the VP (E), and corresponding representative images of EGFP expression (F). Scale bar, 250 μm for all images. L, lateral; D, dorsal.

(G) Nose pokes and cocaine infusions during FR1, FR3, and PR of cocaine self-administration. n = 17, 17, and 16 mice for Ctrl, DRD3 shRNA, DRD3 rescue.

(H) Active and inactive nose pokes during the day 25 seeking test (2 h), corresponding to mice in (G). Active nose pokes were significantly reduced by VP DRD3 KD and restored by DRD3 rescue. Two-way RM ANOVA, Tukey's post hoc test, ***$p < 0.001$; n = 16, 17, and 16 mice for Ctrl and DRD3 shRNA, and DRD3 rescue. Error bars indicate ± SEM for all. See Table S2 for detailed statistics. See also Figure S1.

et al., 2015). Using fluorescent *in situ* hybridization, we found that ∼42.2% ± 2.3% of *NeuN*-expressing cells in the VP co-express *DRD3* (Figures 2A and 2B), indicating that a substantial fraction of VP neurons are likely to signal through DRD3. To understand the extent to which DRD3 signaling in the VP occurs in conjunction with other DA receptors, we quantified the proportion of *DRD3*⁺ VP cells co-expressing *DRD1* or *DRD2* and found that 40.9% ± 3.6% of these cells express neither *DRD1* nor *DRD2* (Figures S2A and S2B). In contrast, in the NAc medial core/shell, we found that all *DRD3*⁺ cells co-express *DRD1* and/or *DRD2*, with a large majority (78.7% ± 1.5%) co-expressing *DRD1* (Figures S2C and S2D). These findings suggest the presence of a

distinct DRD3 signaling landscape in the VP as compared to the NAc medial core/shell. In addition, we found that 68.0% ± 2.2% of VP *DRD3*⁺ cells express *VGAT*, 23.9% ± 2.2% express *VGluT2*, and 6.2% ± 0.8% express *ChAT* (Figures S2E–S2H), suggesting a primarily inhibitory output to downstream structures.

Context- and DRD3-dependent augmented activity of VP DRD3⁺ neurons drives relapse to cocaine seeking

To understand how the activity of DRD3-expressing neurons in the VP is regulated by cocaine, relapse to cocaine seeking, and DRD3 signaling, we virally expressed Cre-dependent
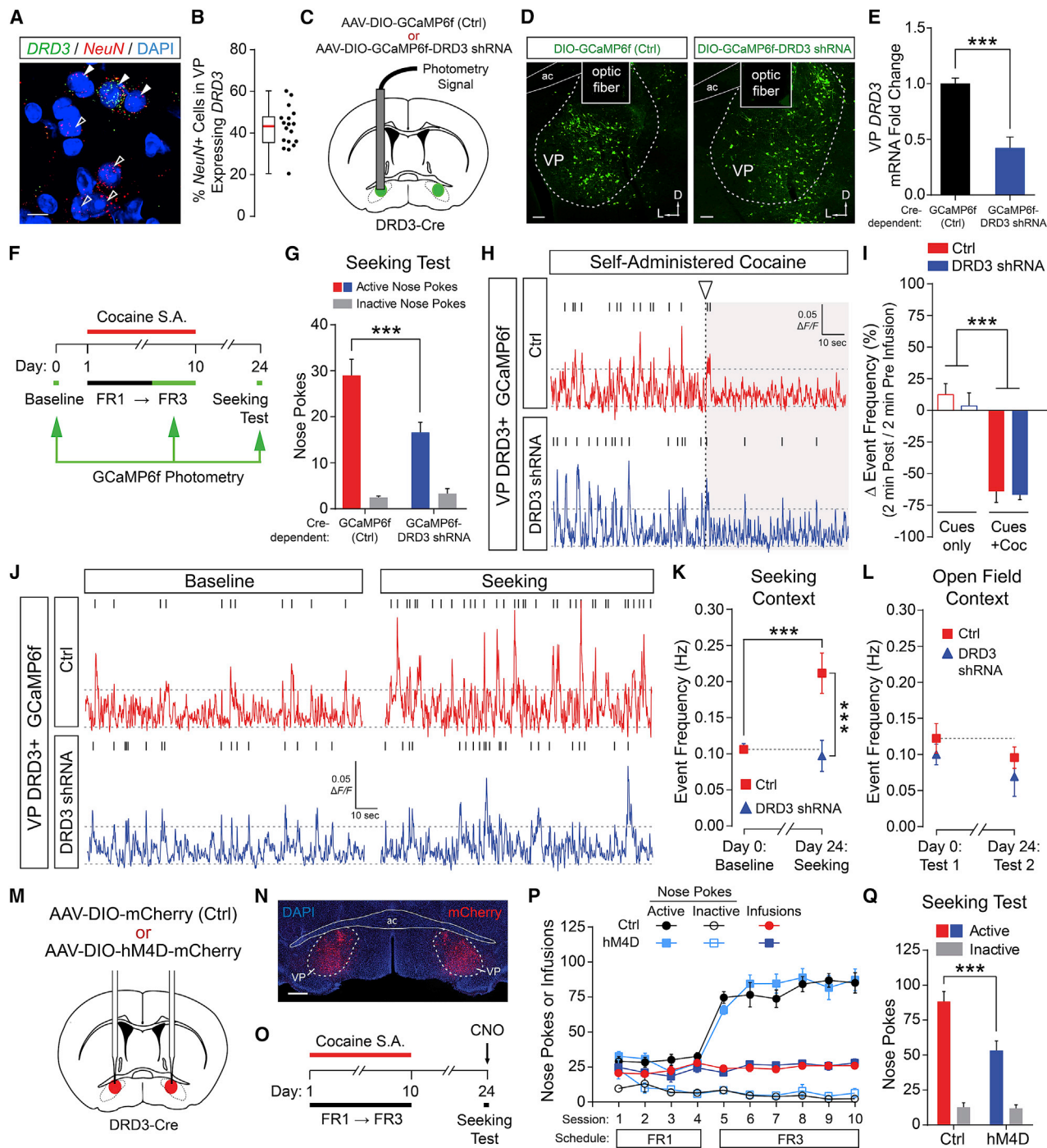
Figure 2. DRD3-dependent augmented activity in the VP drives relapse to cocaine seeking

(A and B) Sample image of RNA *in situ* hybridization (A), and corresponding quantification of *DRD3*+ cells as a percentage of *NeuN*+ cells in the VP (B). Filled arrowheads show double-positive cells, and empty arrowheads show *NeuN*+ only cells. n = 18 images. Scale bar, 20 μm.

(C) Schematic of bilateral viral expression (green) of Cre-dependent GCaMP6f or GCaMP6f-DRD3 shRNA in the VP of DRD3-Cre mice, with unilateral optic fiber implant for photometry.

(D) Sample images of Cre-dependent GCaMP6f and GCaMP6f-DRD3 shRNA expression in the VP, with optic fiber implants. Scale bars, 100 μm. L, lateral; D, dorsal.

(E) Robust KD of *DRD3* expression in the VP of DRD3-Cre mice by Cre-dependent GCaMP6f-DRD3 shRNA. Two-tailed t test, ***p < 0.001, n = 7 mice each for Ctrl and DRD3 shRNA.

(legend continued on next page)

GCaMP6f or GCaMP6f-DRD3 shRNA in the VP of DRD3-Cre mice and used fiber photometry to perform *in vivo* Ca^{2+} imaging (Figures 2C, 2D, S3K, and S3L). We validated DRD3-Cre mice as faithfully recapitulating endogenous *DRD3* expression in the VP (Figures S2I and S2J) and observed a robust KD of *DRD3* expression in the VP using our Cre-dependent GCaMP6f-DRD3 shRNA construct (Figure 2E). This approach allowed us to measure the activity of VP DRD3$^+$ neurons with knocked-down *DRD3* expression while also recapitulating the behavioral effect of reduced cocaine seeking following 2 weeks of abstinence from cocaine self-administration (Figures 2F and 2G).

We found that self-administered intravenous cocaine infusion profoundly reduced the frequency of Ca^{2+} transient events observed during a 2-min period following drug delivery, suggesting a decrease in the average neuronal activity of VP DRD3$^+$ neurons (Figures 2H and 2I). However, when the tone-light cues accompanying successful schedule completion were delivered in the absence of cocaine infusion, the overall Ca^{2+} event frequency of VP DRD3$^+$ neurons was not suppressed (cues only; Figure 2I). Furthermore, these measurements were not significantly altered by VP DRD3 KD, suggesting that DRD3 signaling does not overtly regulate the acute pharmacological effects of cocaine on VP DRD3$^+$ neuronal activity.

In contrast, the frequency of Ca^{2+} events was strongly elevated during the seeking test performed following 2 weeks of home-cage abstinence (day 24) as compared to baseline (day 0) measurements taken in the operant box 1 day prior to the first self-administration session (Figures 2J and 2K). This effect was observed only upon re-exposure to the drug-taking operant context during the seeking test and not in a drug-neutral open field context (Figure 2L) or in drug-naive mice (Figures S3E and S3F). Crucially, DRD3 KD completely abolished the elevated activity observed during cocaine seeking (Figure 2J and 2K), indicating that emergence of drug-salience-encoding activity in the VP requires DRD3 signaling.

To understand the dynamics of VP DRD3$^+$ activity associated with drug-seeking nose pokes, we quantified the area under the curve (AUC) of GCaMP6f signal epochs between −1 s and +3 s surrounding nose pokes (Figures S3A–S3C). Control mice had

significantly higher active nose poke AUC values compared to VP DRD3 KD mice, as well as higher AUC values associated with active nose pokes compared to inactive nose pokes (Figure S3C). However, when plotting the difference in Ca^{2+} event frequency between the baseline (day 0) and the seeking session (day 24) as a function of the number of active nose pokes performed during the seeking session, we observed that for the majority of control mice, the increase in Ca^{2+} events was largely unaccounted for by the number of active nose pokes (Figure S3D, control points above the identity line), suggesting that other aspects of the drug-associated context of the operant box may be strongly evoking VP DRD3$^+$ activity. Furthermore, we performed CPP experiments with VP DRD3$^+$ GCaMP6f photometry, which also showed that VP DRD3$^+$ neuronal activity was significantly elevated in cocaine-treated control mice as compared to VP DRD3 KD mice and saline-treated mice, but only during the preference test that followed a 10-day drug-free period (Figures S3G–S3J). Together, these results suggest that prolonged abstinence elevates VP DRD3$^+$ neuronal activity encoding drug-related contextual salience in a DRD3-dependent manner.

In *ex vivo* patch-clamp experiments following 2 weeks of abstinence from cocaine self-administration, VP DRD3$^+$ neurons showed a DRD3-dependent elevation of intrinsic excitability at high input current steps, increased excitation to inhibition ratio (E:I), and higher resting membrane potential (Figures S4A–S4I), suggesting that VP DRD3$^+$ neurons are primed to augment their response to drug-related inputs following prolonged abstinence.

To determine whether the activity of VP DRD3$^+$ neurons contributes to cocaine-seeking behavior, we bilaterally expressed Cre-dependent Gi-coupled DREADD (hM4D) receptors in the VP of DRD3-Cre mice (Figures 2M and 2N), trained mice to self-administer cocaine for 10 days (Figure 2P), and injected clozapine N-oxide (CNO) 30 min prior to the seeking test on day 24 (Figure 2O). The mice expressing hM4D in VP DRD3$^+$ neurons showed significantly reduced active nose poking following CNO injection on day 24 (Figure 2Q). However, hM4D-mediated suppression of VP DRD3$^+$ activity on day 8 of the consummatory phase did not affect self-administration

---

(F) Experimental schedule of cocaine self-administered experiments with GCaMP6f photometry recording sessions (green arrows) at day 0 (baseline), days 6–10 (FR3), and day 24 (seeking test).

(G) Active and inactive nose pokes during the day 24 seeking test (20 min), corresponding to mice in (C)–(K). Two-way RM ANOVA, Sidak's post hoc test, ***$p < 0.001$; n = 9, 10 mice for Ctrl and DRD3 shRNA.

(H) Sample photometry traces from Ctrl and DRD3 shRNA GCaMP6f constructs expressed in VP DRD3$^+$ neurons. Arrowhead and vertical dotted line indicate the start of a self-administered cocaine infusion. Tick marks above traces indicate threshold-detected events.

(I) Self-administered cocaine infusion decreased activity of VP DRD3$^+$ neurons (cues + Coc), as compared to self-administered cocaine-delivery-associated cues presented in the absence of drug infusion (cues only). Two-way RM ANOVA, main effect$_{cocaine}$ ***$p < 0.0001$; n = 5, 6 mice for Ctrl and DRD3 shRNA.

(J) Sample VP DRD3$^+$ GCaMP6f photometry traces during Baseline versus seeking test sessions, comparing Ctrl and DRD3 shRNA mice. Tick marks above traces indicate threshold-detected events.

(K) DRD3-dependent increase in activity of VP DRD3$^+$ neurons during cocaine seeking. Two-way RM ANOVA, Sidak's post hoc tests, ***$p < 0.001$; n = 9, 10 mice for Ctrl and DRD3 shRNA.

(L) Unaltered VP DRD3$^+$ neuron activity in a drug-free open field context for mice that self-administered cocaine. n = 3, 4 mice for Ctrl and DRD3 shRNA.

(M) Schematic of bilateral viral expression (red) of Cre-dependent mCherry or hM4D-mCherry in the VP of DRD3-Cre mice.

(N) Sample image of bilateral Cre-dependent mCherry expression in the VP of DRD3-Cre mice. Scale bar, 500 μm.

(O) Experimental schedule of cocaine self-administered experiments with CNO administration prior to the seeking test on day 24.

(P) Cocaine self-administration data corresponding to experiments described in (M), (O), and (Q). n = 8 mice each for Ctrl and hM4D.

(Q) hM4D-dependent reduction of VP DRD3$^+$ neuron activity reduces cocaine seeking. Two-way RM ANOVA, Sidak's post hoc test, ***$p < 0.001$; n = 8 mice each for Ctrl and hM4D.

Error bars indicate ± SEM for all. See Table S2 for detailed statistics. See also Figures S2–S4.
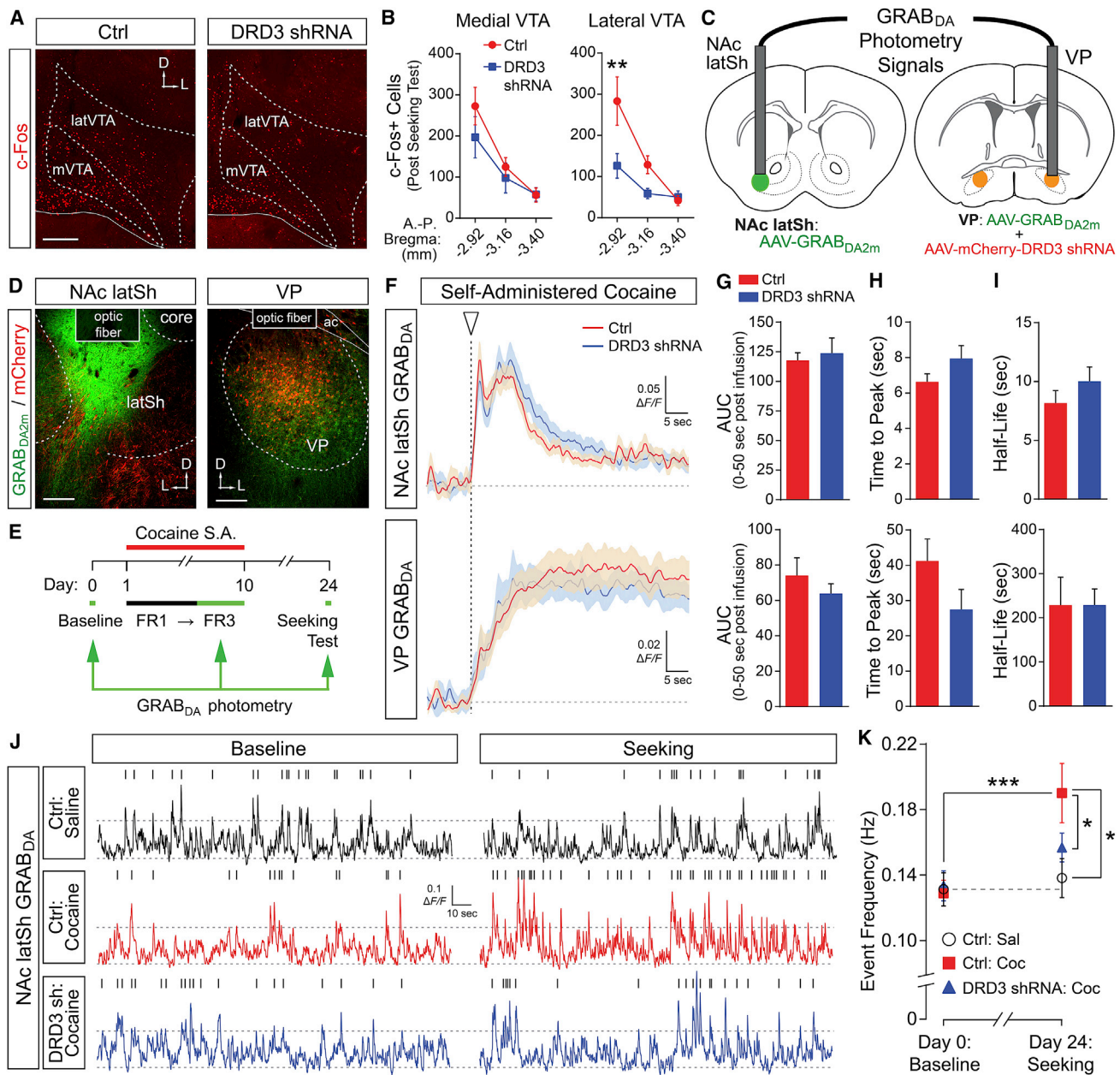
Figure 3. VP DRD3-mediated potentiation of DA release in the NAc latSh during relapse to cocaine seeking

(A) Representative images of c-Fos immunostaining in the VTA of mice that underwent the post-abstinence cocaine-seeking test prior to perfusion, with AAV-mediated bilateral expression of Ctrl or DRD3 shRNA constructs in the VP. Medial VTA (mVTA), lateral VTA (latVTA). Scale bar, 250 μm.

(B) Quantification of the number of c-Fos$^+$ cells in the medial and lateral VTA along anterior-posterior (A.-P.) coordinates, from mice corresponding to (A). Two-way ANOVA, Sidak's post hoc test, **$p < 0.01$ for latVTA A.P. -2.92 Ctrl versus DRD3 shRNA; n = 4–6 images per group.

(C) Schematic of unilateral AAV-GRAB$_{DA2m}$ expression in the NAc latSh and bilateral AAV-GRAB$_{DA2m}$ plus AAV-DRD3 shRNA in the VP, with corresponding optic fibers for photometry.

(D) Sample images of GRAB$_{DA2m}$ and mCherry expression in the NAc latSh and VP. Scale bars, 200 μm. L, lateral; D, dorsal.

(E) Experimental schedule of cocaine self-administered experiments with GRAB$_{DA2m}$ photometry signal collection points (green arrows) at day 0 (baseline), days 6–10 (FR3), and day 24 (seeking test).

(F) Averaged GRAB$_{DA2m}$ photometry signals from NAc latSh (top) and VP (bottom) of Ctrl and VP DRD3 shRNA mice, in response to a self-administered cocaine infusion (arrowhead and vertical dotted line).

(G–I) DA levels in the NAc latSh and VP were indistinguishable between Ctrl and VP DRD3 shRNA following a self-administered cocaine infusion. n = 8, 7 mice for Ctrl and DRD3 shRNA.

(J) Representative traces of NAc latSh GRAB$_{DA2m}$ photometry during baseline (day 0) and seeking test (day 24) sessions. Tick marks above traces indicate threshold-detected events.

(legend continued on next page)

Neuron
Article

behavior (Figures S4J–S4L). In addition, CNO injection did not significantly alter locomotor activity or open field anxiety in hM4D mice (Figures S4M and S4N). Thus, taken together, our results suggest that a DRD3-signaling-induced increase in VP DRD3^{+} neuronal activity drives the process of relapse to cocaine seeking after prolonged abstinence by contributing to the development of contextually specific augmented activity in the VP.

VP DRD3-mediated potentiation of DA release in the NAc latSh during relapse to cocaine seeking

VTA DA neuronal activity and NAc DA release are elevated during cocaine seeking and functionally contribute to relapse to cocaine seeking (Mahler et al., 2019; Phillips et al., 2003; Saunders et al., 2013; Solecki et al., 2020). Moreover, distinct VTA activity and NAc DA release profiles (Liu et al., 2020), as well as distinct functional roles (Bossert et al., 2007; Liu et al., 2020), have been documented across the lateral and medial aspects of the mesolimbic pathway during context-dependent drug relapse. To assess whether VP DRD3 KD may reduce relapse to cocaine seeking by reducing VTA activity relative to control mice seeking cocaine, we quantified c-Fos expression in the latVTA and medial VTA 1 h after the drug-seeking test (Figures 3A and 3B). Strikingly, the rostral latVTA, which projects to the NAc latSh (Yang et al., 2018), showed a pronounced decrease in c-Fos^{+} cells in VP DRD3 KD mice following the seeking test (Figure 3B). This suggests that activity of NAc-latSh-projecting VTA neurons, potentially including DAergic neurons, may be reduced during cocaine seeking in mice with DRD3 KD in the VP.

To measure DA levels in the NAc latSh and VP, we used fiber photometry to perform *in vivo* DA imaging using the genetically encoded DA sensor GRAB$_{DA2m}$ (Sun et al., 2020) (Figures 3C–3E, S5J, and S5K). We first compared the effects of a self-administered intravenous cocaine infusion on DA levels in the NAc latSh versus the VP. In both control and VP DRD3 KD mice, we found that a self-administered cocaine infusion caused DA levels to rapidly rise and decay in the NAc latSh, whereas VP DA levels rose comparatively slowly but persisted at high levels for far longer (Figures 3F to 3I). This suggests a sustained level of DA receptor signaling in the VP during cocaine self-administration sessions, which may cause pronounced effects on local neuronal plasticity.

Throughout GRAB$_{DA2m}$ imaging sessions, we observed frequent transient events in the NAc latSh signal. During the seeking test, we expected a substantial fraction of these events to represent motivational drive and reward expectation previously associated with the cocaine self-administration context during the consummatory phase (de Jong et al., 2019; du Hoffmann and Nicola, 2014; Phillips et al., 2003; Roitman et al., 2004). We quantified the average frequency of DA transient events occurring during the pre-drug baseline (day 0) and seeking (day 24) imaging sessions in control and VP DRD3 KD mice that had previously self-administered saline or cocaine

(Figure 3J). Whereas the frequency of DA transients in the NAc latSh of control mice was significantly elevated during the seeking test as compared to the pre-drug baseline, VP DRD3 KD mice seeking cocaine, as well as saline controls, did not show a significant elevation in the frequency of DA transients during the seeking test (Figures 3J and 3K).

To assess NAc latSh DA release associated with cocaine-seeking nose pokes, we quantified AUC for GRAB$_{DA2m}$ signal epochs between −1 s and +3 s surrounding nose pokes (Figures S5A–S5D). We divided our analysis into two parts, separating the first 50% of nose pokes from the second 50% of nose pokes performed by each animal during the seeking test, as we expected a gradual devaluation of active nose pokes over the course of the seeking test. Similar to VP DRD3^{+} GCaMP6f recordings, control mice had higher AUC values associated with active nose pokes compared to inactive nose pokes; however, these effects were only statistically significant for the first 50% of nose pokes performed during the seeking session (Figure S5C, 0–50, nose-poke-type main effect). In addition, when analyzing active nose-poked-related events aggregated from all subjects (using subject ID as a covariate), control mice had higher active-nose-poke GRAB$_{DA2m}$ AUC values than VP DRD3 KD mice, for the first 50% of active nose pokes performed (Figure S5D, 0–50). Analogous analyses of GRAB$_{DA2m}$ measurements from the VP indicated similar but less robust trends compared to the NAc latSh (Figures S5E–S5H). Furthermore, as for VP DRD3^{+} GCaMP6f recordings, for control mice that self-administered cocaine, we found that the increase in number of DA release events occurring across the seeking session (day 24) as compared to the pre-drug baseline (day 0) was generally larger than the number of active nose pokes performed during the seeking session (Figure S5I, control points above the identity line), suggesting that elevated DA release in the NAc latSh is not simply a function of active nose pokes performed. Taken together, this set of results strongly suggests that DRD3-dependent signaling in the VP contributes to elevating accumbal DA release during relapse to cocaine seeking.

VP DRD3^{+} neuronal projections to the LHb and VTA are predominantly inhibitory

To understand the circuit-level mechanisms through which VP DRD3^{+} neurons control DA release in the NAc, we probed the anatomical and functional properties of VP DRD3^{+} neuronal projections to the LHb and VTA, as these two targets have been previously shown to control reward-related behaviors (Faget et al., 2018; Knowland et al., 2017; Stephenson-Jones et al., 2020). VP DRD3^{+} neurons send non-collateralizing, synapse-forming projections to the LHb and VTA (Figures S6A–S6F and 4A–4D). Whole-cell patch-clamp recordings from the LHb and VTA revealed large ChR2-evoked GABA$_A$-receptor-mediated responses in both target structures, with small and infrequent

(K) Ctrl mice seeking cocaine have a significantly higher number of DA release events in the NAc latSh as compared to their baseline event frequency, as well as compared to VP DRD3 shRNA mice seeking cocaine or Ctrl mice that self-administered saline. Two-way RM ANOVA, Sidak's post hoc tests comparing baseline versus seeking days, ***$p < 0.001$; Newman-Keuls post hoc tests comparing treatments, *$p < 0.05$; n = 6, 10, and 9 mice for Ctrl:Sal, Ctrl:Coc, and DRD3 shRNA:Coc.

Error bars or shading indicate ± SEM for all. See Table S2 for detailed statistics. See also Figure S5.
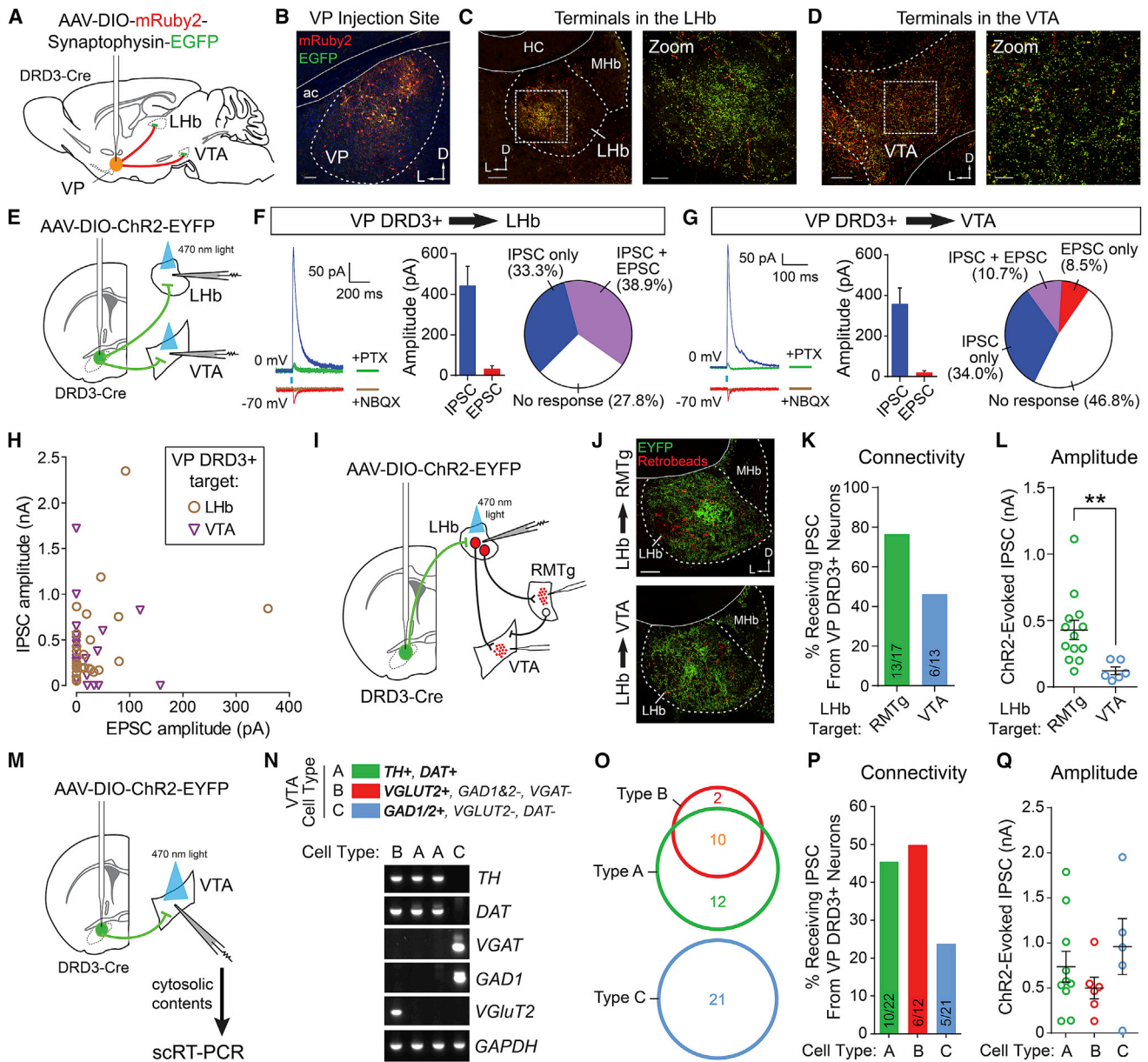
Figure 4. Characterization of VP DRD3+ projections to the LHb and VTA

(A and B) Cre-dependent AAV-mRuby2/synaptophysin-EGFP was stereotaxically injected in the VP of DRD3-Cre mice to visualize synaptic terminals in the LHb and VTA. Scale bar, 100 μm. L, lateral; D, dorsal.

(C and D) Representative images showing a high density of VP DRD3+ synaptic terminals in the LHb and VTA. Scale bars represent 100 μm for left panels and 30 μm for right (zoom) panels.

(E) Schematic of Cre-dependent ChR2 expression in the VP of DRD3-Cre mice to characterize connectivity to the LHb and VTA using whole-cell patch-clamp electrophysiology.

(F and G) Large IPSCs and some small excitatory postsynaptic currents (EPSCs) were evoked by stimulating ChR2-expressing VP DRD3+ terminals in the LHb or VTA. Bar graphs show average IPSC and EPSC amplitudes for connected cells. Pie charts indicate percent connectivity for each type of response. n = 26/36 and 25/47 connected/total cells patched from LHb and VTA. PTX, picrotoxin, GABA$_A$R antagonist; NBQX, AMPA/kainate receptor antagonist.

(H) Scatterplot of ChR2-evoked IPSC versus EPSC amplitudes for VP DRD3+ neurons projecting to the LHb or VTA.

(I) Schematic for experiments assessing connectivity of VP DRD3+ neurons to LHb neurons projecting to the RMTg or VTA; Cre-dependent ChR2 expression in the VP of DRD3-Cre mice, with red retrobeads injected in the RMTg or VTA.

(J) ChR2-EYFP-expressing terminals and red retrobeads in the LHb, corresponding to experiments in (I), (K), and (L). Scale bar represents 100 μm for both images.

(K) IPSC connectivity of VP DRD3+ neurons to LHb neurons targeting the RMTg or VTA. Connected/total cells.

(L) ChR2-evoked IPSC amplitudes corresponding to connected cells in (K). Mann-Whitney two-tailed U test, **p = 0.002.

(legend continued on next page)

Neuron
Article

contributions from AMPA-receptor-mediated currents (Figures 4E–4H). Connectivity was higher in the LHb (72.2%) than the VTA (53.2%), suggesting greater control over LHb output. The LHb is known to provide excitatory input to GABAergic neurons of the VTA and rostromedial tegmental nucleus (RMTg) (Araki et al., 1988; Brinschwitz et al., 2010), which in turn inhibit VTA DA neurons (Hong et al., 2011; Ji and Shepard, 2007; Lammel et al., 2012). To determine whether VP DRD3+ neurons connect to this circuit, we recorded VP DRD3+ ChR2-evoked inhibitory post-synaptic currents (IPSCs) from LHb neurons labeled by red retrobeads injected in the VTA or RMTg (Figures 4I and 4J). Both connectivity and the amplitude of ChR2-evoked IPSC responses were greater for LHb neurons projecting to the RMTg (Figures 4K and 4L), suggesting that LHb-projecting VP DRD3+ neurons may disinhibit VTA DA neurons primarily via RMTg GABAergic neurons.

To characterize the cell-type-specific connectivity of VP DRD3+ neurons sending direct projections to the VTA, we used single-cell RT-PCR (scRT-PCR) to identify genetic markers of cells receiving ChR2-evoked IPSCs directly from VP DRD3+ neurons (Figures 4M and 4N). We categorized patched VTA cells as putatively DAergic (type A), glutamatergic (type B), or GABAergic (type C) and found substantial overlap between type A and type B cells (Figures 4N and 4O). Putatively GABAergic VTA cells (type C) received approximately half as many inhibitory inputs from VP DRD3+ neurons as putatively DAergic (type A) and glutamatergic (type B) VTA cells (23.8% versus 45.5% and 50.0%, respectively), but IPSC amplitudes were similar across all three categories (Figures 4P and 4Q). Therefore, VTA-projecting VP DRD3+ neurons may have the capacity to excite or inhibit DAergic neurons depending on which subsets of cells are activated and/or depending on their firing pattern. On the other hand, LHb-projecting VP DRD3+ neurons are likely to inhibit LHb neurons projecting to GABAergic midbrain neurons, thereby disinhibiting mesoaccumbal DA neurons (Barrot et al., 2012; Brown et al., 2017; Lammel et al., 2012).

Optogenetic stimulation of VP DRD3+ neuronal projections to the LHb and VTA causes DA release in the NAc latSh and appetitive behavior

To assess the ability of distinct VP DRD3+ neuronal projections to alter accumbal DA release, we monitored GRAB_DA2m activation in the NAc latSh in response to ChR2-mediated stimulation of VP DRD3+ neuronal projections to the LHb or VTA (Figures 5A, 5F, S7A–S7C, and S7F–S7H). We found that stimulation of both LHb- and VTA-projecting VP DRD3+ neurons elevated DA

release in the NAc latSh during stimulation periods (Figures 5B, 5C, 5G, 5H, S7D, and S7E), suggesting that concerted, artificial activation of either projection can drive appetitive behavior. Indeed, contextually paired stimulation of either LHb- or VTA-projecting VP DRD3+ neurons drove real-time place preference (Figures 5D, 5E, 5I, and 5J).

Activity of VP DRD3+ axonal terminals in the LHb is augmented during relapse to cocaine seeking

To understand the relative contributions of LHb-projecting versus VTA-projecting VP DRD3+ neurons to relapse to cocaine seeking after abstinence, we first directly monitored the activity of each projection at baseline (day 0) and during the cocaine-seeking test (day 24) using viral-mediated delivery of axon-targeting GCaMP6s to VP DRD3+ neurons (Broussard et al., 2018) and fiber photometric measurements of axonal Ca2+ signals from each target structure (Figure 6A, S7I, and S7J). The overall frequency of Ca2+ signal transients in axonal terminals of VP DRD3+ neurons in the LHb was significantly elevated during the post-abstinence seeking test as compared to baseline levels, whereas Ca2+ signals in axonal terminals of VP DRD3+ neurons in the VTA did not differ significantly between the two sessions (Figures 6B and 6C). Interestingly, unlike our findings from VP DRD3+ GCaMP6f recordings, AUC for the −1 s to +3 s time window surrounding nose pokes was not significantly different between active and inactive nose pokes for either the LHb or VTA terminals (Figures S7K–S7M), suggesting that active nose-poke-related transients may preferentially occur in subpopulations of VP DRD3+ neurons projecting to other targets (e.g., NAc, mediodorsal thalamus [MD], or lateral hypothalamus [LH]). Together, our results suggest that LHb-projecting VP DRD3+ neurons are selectively and tonically activated throughout the cocaine-seeking session and that this activity may be disinhibiting mesoaccumbal DA release to invigorate cocaine-seeking behavior.

The difference between LHb- and VTA-projecting VP DRD3+ neuronal activity during post-abstinence seeking (day 24) may be caused by various factors, including the relative contributions of brain-wide anatomical inputs to each projection branch. Indeed, using monosynaptic rabies tracing combined with target-specific retrograde viral expression of Cre-dependent Flp recombinase (RG-EIAV-DIO-Flp) (Knowland et al., 2017; Lilascharoen et al., 2021) (Figure 6D), we uncovered significant differences in inputs from the NAc latSh, central amygdala (CeA), and basomedial amygdala (BMA) (Figures 6E and 6F),

(M) Schematic showing procedure for collecting cytosolic contents from single VTA neurons receiving monosynaptic inputs from VP DRD3+ neurons, followed by single-cell RT-PCR (scRT-PCR).

(N) Sample images of scRT-PCR products for VTA cell-type markers: TH, tyrosine hydroxylase; DAT, dopamine transporter; VGLUT2, vesicular glutamate transporter 2; GAD1&2, GAD1/2, glutamic acid decarboxylase 1 and 2, 1 or 2; VGAT, vesicular GABA transporter. Cell type "A" was defined as DAergic-like based on expression of both TH and DAT, cell type "B" was defined as glutamatergic-like based on expression of VGLUT2 and absence of GAD1&2 and VGAT, and cell type "C" was defined as GABAergic-like based on expression of GAD1 or 2 and absence of VGLUT2 and DAT.

(O) Total number of cells recorded and genetically characterized for each of the three cell types presented in (N), (P), and (Q).

(P) Percentage of VTA cell types A, B, and C receiving IPSC input from VP DRD3+ neurons. Connected/total cells.

(Q) ChR2-evoked IPSC amplitudes corresponding to connected cells in (P).

Error bars indicate ± SEM for all. See Table S2 for detailed statistics. See also Figure S6.
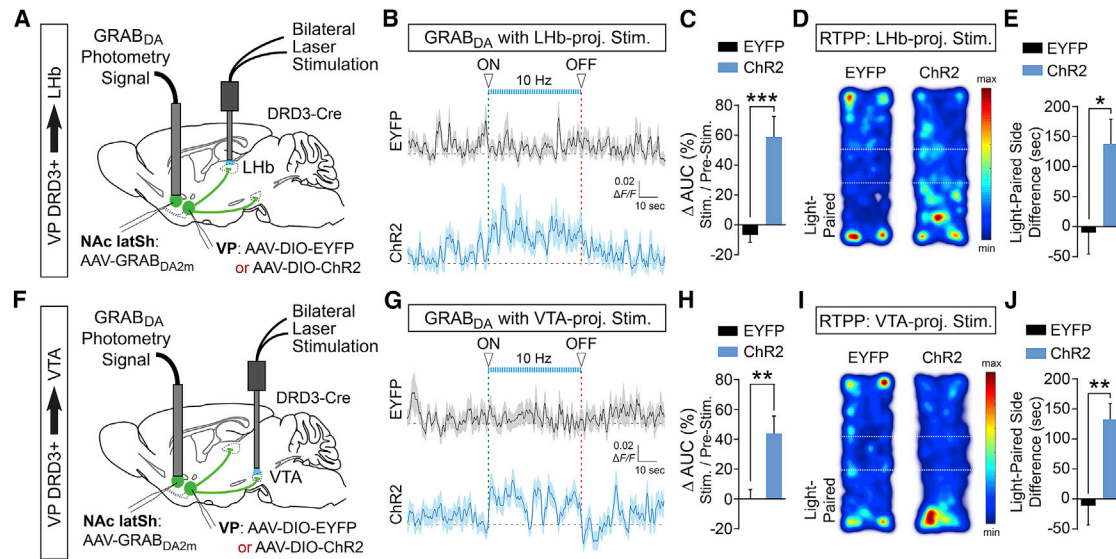
Figure 5. VP DRD3+ projections to the LHb and VTA Ctrl NAc latSh DA release and appetitive behavior

(A and F) Cre-dependent ChR2 or EYFP were expressed in the VP of DRD3-Cre mice and projections to the LHb (A) or VTA (F) were optogenetically stimulated while GRAB$_{DA2m}$ was monitored in the NAc latSh.

(B and C) DA release in the NAc latSh was elevated while stimulating VP DRD3+ terminals in the LHb. Analysis of covariance (ANCOVA) using subject ID (mouse identity) as a covariate, ***p < 0.001; n = 24 and 25 trials for EYFP and ChR2, from four mice each. Analysis by subject presented in Figure S7D.

(D and E) Real-time place preference was induced by optogenetic stimulation of VP DRD3+ terminals in the LHb. Mann-Whitney two-tailed U test, *p = 0.045; n = 8 and 5 mice for EYFP and ChR2.

(G and H) DA release in the NAc latSh was elevated while stimulating VP DRD3+ terminals in the VTA. ANCOVA using subject ID as a covariate, **p = 0.003 for treatment comparison; n = 28 and 34 trials for EYFP and ChR2, from four mice each. Analysis by subject presented in Figure S7E.

(I and J) Real-time place preference was induced by optogenetic stimulation of VP DRD3+ terminals in the VTA. Mann-Whitney two-tailed U test, **p = 0.002; n = 7 and 11 mice for EYFP and ChR2.

Error bars indicate ± SEM for all. See Table S2 for detailed statistics. See also Figure S7.

supporting a distinction between the functional roles of LHb- and VTA-projecting VP DRD3+ neurons.

Activity and DRD3 expression in LHb-projecting VP DRD3+ neurons is necessary to drive relapse to cocaine seeking

To further address the relative functional contributions of LHb- and VTA-projecting VP DRD3+ neurons during relapse to cocaine seeking, we first optogenetically or chemogenetically manipulated terminal activity of VP DRD3+ neurons during the post-abstinence seeking test (day 24) using bilateral optic fibers or drug-infusion cannulae positioned above each target structure (Figures 7A, 7F, S8A, and S8B). We found that inhibiting VP DRD3+ neuronal terminals in the LHb, either episodically with Cre-dependent NpHR3.0 or throughout the seeking test with Cre-dependent hM4D, significantly reduced the number of active nose pokes performed during the seeking test, whereas episodic ChR2-mediated activation of this projection had no effect on nose poke number (Figures 7B–7E). Conversely, optogenetically activating or inhibiting VP DRD3+ terminals in the VTA did not significantly alter nose pokes performed during the seeking session, whereas hM4D-mediated inhibition throughout the seeking test slightly elevated the number of both active and inactive nose pokes performed, suggesting a small increase in either overall locomotor activity or motivated drug seeking

when using uninterrupted inhibition of activity throughout the session (Figures 7G–7J).

Second, we assessed cocaine-seeking behavior in groups of mice with *DRD3* expression knocked down in either the LHb- or the VTA-projecting subpopulations of VP neurons. We achieved this by using a Cre-dependent *DRD3* KD construct virally expressed in the VP, combined with a retrograde Cre-expressing virus (RG-EIAV-Cre) (Knowland et al., 2017; Lilaschar-oen et al., 2021) injected either in the LHb or the VTA (Figure 7K and 7L). Consistent with previous findings for VP PV+ neurons (Knowland et al., 2017) and our findings for VP DRD3+ neurons (Figure S6), we found that LHb-projecting and VTA-projecting VP neurons form distinct subpopulations that show minimal axonal cross-collateralization (Figure 7L), enabling us to separately manipulate DRD3 expression in each projection branch. Strikingly, DRD3 KD in LHb-projecting VP neurons reduced the number of active nose pokes performed during the post-abstinence seeking test (day 24), while DRD3 KD in VTA-projecting VP neurons had no effect. Thus, on the whole, our findings support the conclusion that augmented activity of LHb-projecting VP DRD3+ neurons by cocaine-associated contextual cues drives relapse to cocaine-seeking behavior and that DRD3-dependent plasticity within the LHb-projecting branch of the VP plays a critical role in driving cocaine-seeking behavior.
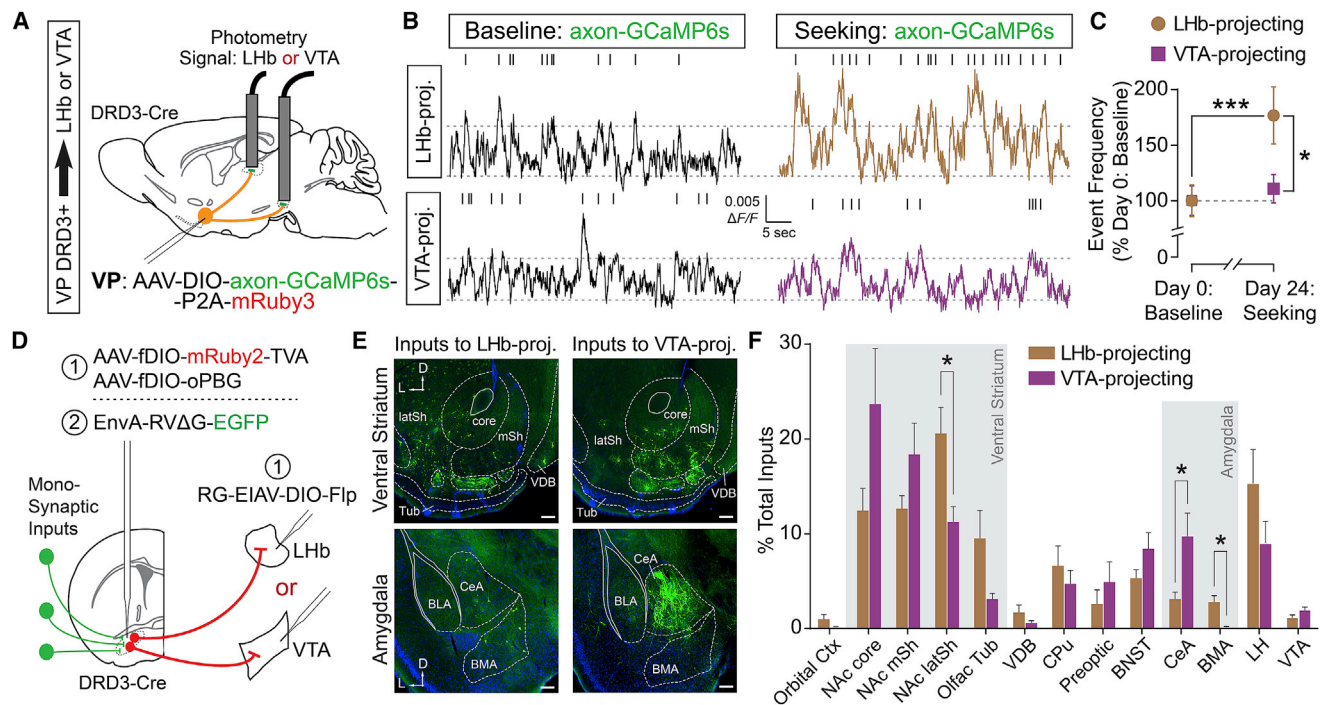
Figure 6. Augmented activity of VP DRD3$^+$ axonal terminals in the LHb during relapse to cocaine seeking

(A) Cre-dependent axon-targeting GCaMP6s was expressed in the VP of DRD3-Cre mice and fiber photometry signals were collected from VP DRD3$^+$ terminals in the LHb and VTA.

(B) Representative photometry signal traces collected from VP DRD3$^+$ axonal terminals in the LHb (top panels) or VTA (bottom panels) at baseline (left panels) or during post-abstinence cocaine seeking (day 24) (right panels). Tick marks above traces indicate threshold-detected events.

(C) Activity of VP DRD3$^+$ axonal terminals in the LHb was significantly elevated during the seeking test compared to their baseline levels, as well as compared to the activity of VP DRD3$^+$ axonal terminals in the VTA. Two-way RM ANOVA, Sidak's post hoc tests, *p < 0.05, ***p < 0.001; n = 7 mice each for LHb and VTA.

(D) Schematic of viral strategy to identify monosynaptic inputs to LHb- or VTA-projecting VP DRD3$^+$ neurons. DRD3-Cre mice were (1) injected with Flp-dependent TVA and oPBG-expressing viruses in the VP and Cre-dependent Flp recombinase-expressing retrograde equine infectious anemia virus (RG-EIAV-DIO-Flp) in the LHb or VTA; (2) 3 weeks later, EnvA-pseudotyped rabies virus expressing EGFP was injected in the VP.

(E) Representative images of monosynaptic inputs to LHb- and VTA-projecting VP DRD3$^+$ neurons. Scale bars, 200 μm. L, lateral; D, dorsal.

(F) Quantification of brain-wide inputs to LHb- and VTA-projecting VP DRD3$^+$ neurons. Mann-Whitney two-tailed U tests, *p < 0.05 for NAc latSh, CeA, and BMA; n = 5 and 4 hemispheres each.

Orbital Ctx, orbital cortex; NAc core, nucleus accumbens core; NAc mSh, nucleus accumbens medial shell; NAc latSh, nucleus accumbens lateral shell; Olfac Tub, olfactory tubercle; VDB, vertical diagonal band; CPu, caudate putamen; Preoptic, preoptic area; BNST, bed nucleus of the stria terminalis; CeA, central amygdala; BMA, basomedial amygdala; LH, lateral hypothalamus; VTA, ventral tegmental area.

Error bars indicate ± SEM for all. See Table S2 for detailed statistics. See also Figure S7.
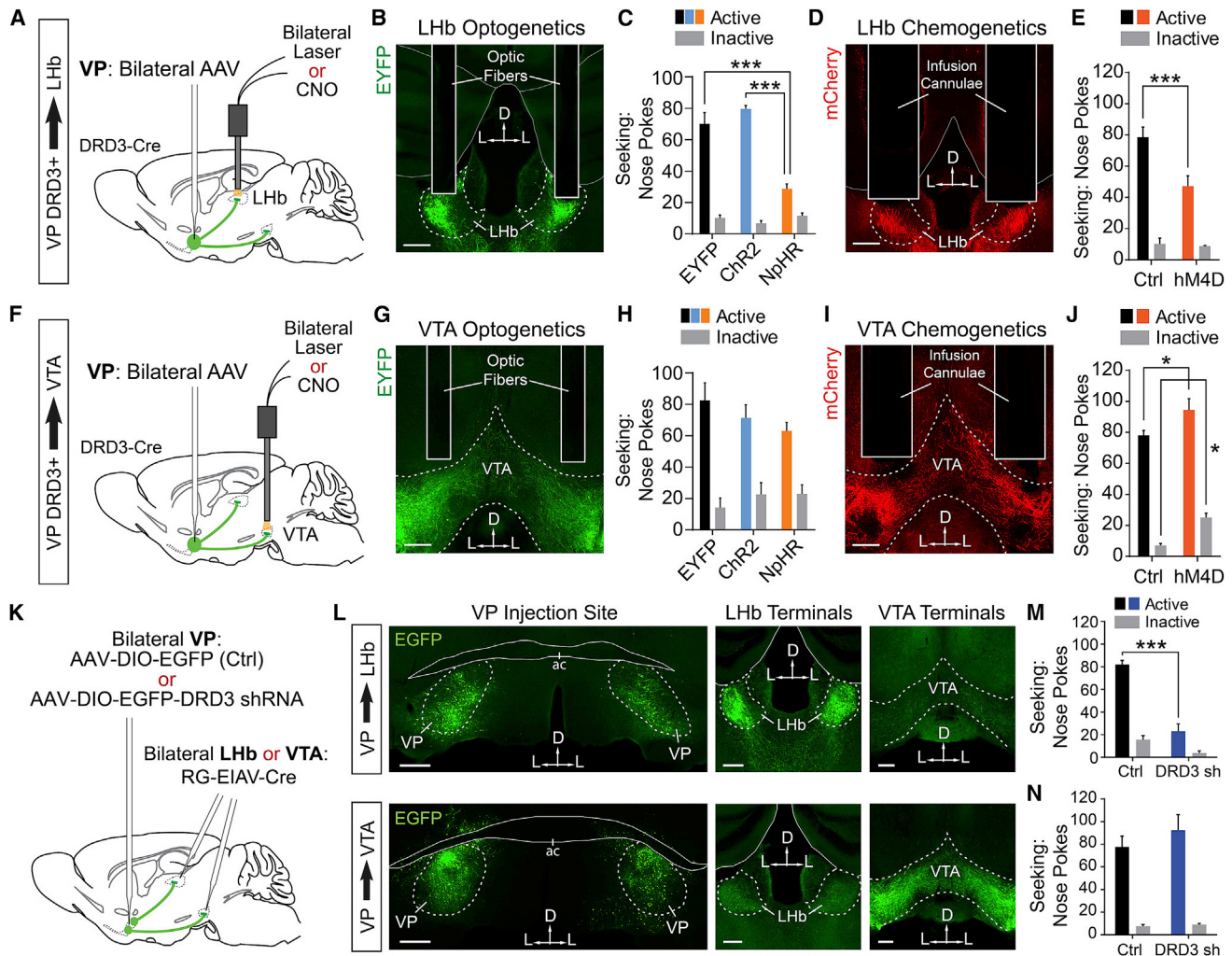
DISCUSSION

Identifying the factors that sustain long-lasting vulnerability to drug relapse is pivotal to designing therapeutics for addictive disorders. Our model incorporates a 2-week period of forced abstinence in the home cage, which is aimed at modeling periods of involuntary drug unavailability in human addiction (Farrell et al., 2018; Reiner et al., 2019; Venniro et al., 2016). In this study, we provide a molecular and circuit-level understanding of how repeated use of cocaine can modify the activity of a subset of neurons in the VP to influence DA release in the NAc and motivate drug seeking upon delayed reexposure to the self-administration context.

DRD3 expression in the VP as a critical factor driving relapse to cocaine seeking

We found that prolonged abstinence from passive or self-administered cocaine elevates *DRD3* expression in the VP. This in-crease parallels gene expression (Freeman et al., 2010; Walker et al., 2018) and DNA methylation (Massart et al., 2015) changes observed in several brain regions, specifically following long (>10 days) periods of abstinence from cocaine self-administration, but not following short (1 day) abstinence. Increased DRD3 expression may be driving augmented activity of VP neurons during relapse, possibly through suppression of inhibitory neurotransmission (Chen et al., 2006; Shin et al., 2018; Swant et al., 2008) or an increase in excitability resembling the effects of DRD2 overexpression (Cazorla et al., 2012).

Pharmacological antagonism of DRD3 signaling has been shown to attenuate various forms of relapse to drug seeking (Andreoli et al., 2003; Galaj et al., 2015; Sokoloff and Le Foll, 2017; Vorel et al., 2002; Xi and Gardner, 2007; Xi et al., 2013). Here, we used a highly specific approach to studying DRD3 function during relapse by selectively knocking down DRD3 expression in the VP, an anatomical reward hub not previously studied in the

Figure 7. Activity and DRD3 signaling in the LHb-projecting branch of VP DRD3$^+$ neurons is necessary to drive relapse to cocaine seeking

(A, B, and D) Cre-dependent AAVs were injected bilaterally in the VP of DRD3-Cre mice, and bilateral optic or drug-infusion cannulae were implanted over the LHb. Scale bars, 200 μm. L, lateral; D, dorsal for all.

(C and E) Mice seeking cocaine following 2 weeks of abstinence performed fewer active nose pokes if VP DRD3$^+$ terminals in the LHb were inhibited with NpHR (C) or with hM4D (E). Two-way RM ANOVA for optogenetic treatment, Tukey's post hoc tests, ***$p < 0.001$; n = 7, 4, and 7 mice for EYFP, ChR2, and NpHR. Two-way RM ANOVA for chemogenetic treatment, Tukey's post hoc test, ***$p < 0.001$; n = 4 and 6 mice for Ctrl and hM4D.

(F, G, and I) Cre-dependent AAVs were injected bilaterally in the VP of DRD3-Cre mice, and bilateral optic or drug-infusion cannulae were implanted over the VTA. Scale bars, 200 μm. L, lateral; D, dorsal for all.

(H and J) Optogenetically stimulating or inhibiting VP DRD3$^+$ terminals in the VTA did not affect cocaine seeking (H), whereas chemogenetically inhibiting VP DRD3$^+$ terminals in the VTA with hM4D significantly elevated both active and inactive nose pokes (J). n = 5, 6, and 7 mice for EYFP, ChR2, and NpHR. Two-way RM ANOVA for chemogenetic treatment, Tukey's post hoc tests, *$p < 0.05$; n = 5 and 5 mice for Ctrl and hM4D.

(K) Schematic for experiments in (L), (M), and (N). Cre-dependent EGFP (Ctrl) or DRD3 shRNA were injected bilaterally in the VP of wild-type mice, and Cre recombinase-expressing RG-EIAV was injected in the LHb or VTA to selectively knock down *DRD3* expression in LHb- or VTA-projecting VP neurons.

(L) Representative images of EGFP expression in LHb-projecting (top panels) or VTA-projecting (bottom panels) VP neurons, showing minimal collateralization between the two projections. Scale bars represent 500 μm for the VP injection site and 200 μm for LHb and VTA terminals. L, lateral; D, dorsal for all.

(M) KD of *DRD3* expression in LHb-projecting VP neurons decreases cocaine seeking following 2 weeks of abstinence from cocaine self-administration (day 24). Two-way RM ANOVA, Sidak's post hoc test, ***$p < 0.001$; n = 3 mice each for Ctrl and DRD3 shRNA.

(N) As in (M), but for VTA-projecting VP neurons. n = 3 mice each for Ctrl and DRD3 shRNA.

Error bars indicate ± SEM for all. See Table S2 for detailed statistics. See also Figure S8.

context of DRD3 function. Consistent with systemic administration of DRD3 antagonists, we found decreased drug seeking in mice with DRD3 KD in the VP. However, whereas systemic DRD3 antagonism reduces cocaine self-administration under high-ratio and PR schedules (Xi and Gardner, 2007; Xi et al., 2005), we found that VP DRD3 KD did not significantly impact FR3 or PR performance, suggesting that VP DRD3-mediated plasticity either plays a larger role under conditions when

Neuron
Article

CellPress
OPEN ACCESS

reinforcement is absent or impacts the development of incubation of cocaine craving (Pickens et al., 2011). Our observations that CPP score and VP DRD3+ neuronal activity in the CPP paradigm are only significantly affected by DRD3 KD after 10 days of abstinence suggest that prolonged abstinence enhances the contribution of VP DRD3 signaling to cocaine seeking.

DRD3 controls augmented activity of VP neurons during relapse

To understand how DRD3 KD in the VP reduces cocaine seeking after abstinence, we explored how DRD3 signaling in the VP impacts neural activity and plasticity. Using *in vivo* Ca^{2+} imaging, we found that activity of DRD3-expressing VP neurons is elevated during the drug-deprived cocaine-seeking state, decreased during the cocaine-intoxicated state, and unaltered in a context never paired with cocaine. Recent findings show a similar increase in the firing rate of VP GABAergic neurons during cue-induced reinstatement of cocaine seeking (Heinsbroek et al., 2020). Augmented activity of VP DRD3+ neurons during cocaine seeking, as well as increased net excitatory drive to these neurons during the abstinence period, were all vitally dependent on DRD3 expression. Mimicking the effects of DRD3 KD by chemogenetically inhibiting VP DRD3+ neuronal activity also resulted in suppressed drug seeking. Together, these findings support the notion that VP DRD3+ neurons encode cocaine craving and drive cocaine seeking in the drug-associated environment in a manner dependent on DRD3-mediated plasticity. How might cocaine induce plasticity in the VP via DRD3 signaling? We observed a large and prolonged increase in DA release in the VP in response to intravenous cocaine infusion. The decay of DA release in the VP displayed a longer half-life than in the NAc latSh, possibly due to lower DRD2-mediated autoregulation of DA release (Mengual and Pickel, 2002) and/or lower DA transporter expression (Stout et al., 2016) in the VP as compared to striatal areas. Thus, despite sparse DAergic innervation of the VP as compared to the NAc (Adrover et al., 2014; Papathanou et al., 2019), DA may play an important local signaling role in the VP in response drugs of abuse, such as cocaine, that cause long-lasting elevation of DA. DRD3 may be especially important given its higher affinity for DA (Richtand, 2006; Robinson et al., 1994; Sokoloff et al., 1990).

Which direct synaptic inputs are modulating VP DRD3+ neuronal activity? Prior work has shown that DRD1-expressing NAc medium spiny neurons (D1 MSNs) increase their activity in response to passively administered cocaine and immediately prior to entry into a drug-associated context, whereas DRD2-expressing NAc medium spiny neurons (D2 MSNs) correspondingly decrease their activity (Calipari et al., 2016). As VP DRD3+ neurons receive a large fraction of their inputs from the ventral striatum, likely from an equal mix of D1 and D2 MSNs (Creed et al., 2016; Knowland et al., 2017), it is possible that elevated D1-MSN-mediated inhibition dominates during the cocaine-intoxicated state, whereas reduced D2 MSN-mediated inhibition during seeking disinhibits VP DRD3+ neurons. Inputs from the VTA are also a probable source of modulation, as glutamatergic VTA neurons synapse onto and activate VP neurons (Yoo et al., 2016), and VTA neuron firing is acutely suppressed by cocaine (Calipari et al., 2017).

Distributed control of NAc latSh DA release via pallido-habenular DRD3+ neurons

Because KD of DRD3 in the VP blocked augmented activity of VP DRD3+ neurons in the cocaine-seeking context, we expected a distributed effect of VP DRD3 KD on neuronal activity in other structures of the reward circuitry, including the VTA. Indeed, we observed reduced activation of neurons in the latVTA and reduced DA release in the NAc latSh of VP DRD3 KD mice during the seeking test. This suggests that VP DRD3+ neurons regulate the reciprocal circuit between latVTA DA neurons and NAc latSh MSNs, a circuit that is known to drive appetitive behavior (Yang et al., 2018) and has been associated with relapse behavior (Bossert et al., 2007; Liu et al., 2020). DA release in the NAc is crucial for expression of cocaine-seeking behavior (Mahler et al., 2019; Phillips et al., 2003; Saunders et al., 2013; Solecki et al., 2020) and generally plays an important role in motivational vigor, reinforcement learning, and reward processing (Hamid et al., 2016; Salamone and Correa, 2012; Schultz, 2016; Watabe-Uchida et al., 2017). We therefore sought to understand how VP DRD3+ neuronal activity regulates DA release in the NAc latSh by dissecting the circuitry connecting VP DRD3+ neurons to the VTA. We compared the direct projection to the VTA with an indirect connection to the VTA sent via the LHb. We found that both LHb-projecting and VTA-projecting VP DRD3+ neurons were primarily GABAergic and capable of eliciting DA release in the NAc latSh and real-time place preference when optogenetically stimulated. The LHb is largely devoid of GABAergic interneurons (Brinschwitz et al., 2010) and sends excitatory projections to inhibitory GABAergic neurons in the VTA and RMTg (Araki et al., 1988; Brinschwitz et al., 2010), thereby inhibiting VTA DA neurons (Hong et al., 2011; Ji and Shepard, 2007; Lammel et al., 2012). We found that VP DRD3+ neurons preferentially inhibited RMTg-projecting LHb neurons. Therefore, we suspect that activation of pallido-habenular VP DRD3+ neurons suppresses LHb activity, which reduces activity in GABAergic RMTg neurons and thereby disinhibits VTA DA neurons, leading to increased DA release in the NAc latSh. On other hand, because we observed that VTA-projecting VP DRD3+ neurons synapse onto both DAergic and GABAergic neurons in the VTA, it is unclear precisely how these predominantly inhibitory VP DRD3+ neurons elicit DA release in the NAc latSh. It appears that strong and concerted activation of VP DRD3+ projections to the VTA using ChR2 results in a net disinhibition of VTA DA neurons. However, natural forms of activity may select for subsets of VP DRD3+ neurons projecting only to VTA DA neurons or only to VTA GABA neurons during specific behaviors, which could result in net excitation or inhibition of VTA DA neurons.

Our axonal fiber photometry measurements showed that LHb-projecting VP DRD3+ neurons tonically elevate their activity during drug seeking after abstinence, whereas the VTA-projecting branch does not. Thus, elevated activity inferred from our somatic measurements of VP DRD3+ neurons (Figure 2) would be expected to contain the elevated activity of neurons projecting to the LHb and possibly other subpopulations not explored in this study, such as those projecting to the NAc, MD, or LH. Compared to the VTA-projecting population, LHb-projecting VP DRD3+ neurons received more direct input from the NAc latSh and BMA but less input from the CeA (Figure 6). DA is

released in the NAc latSh in response to reward and reward-predictive cues (de Jong et al., 2019; Liu et al., 2020), and inhibition of the NAc latSh to VP projection regulates motivational attraction to reward-paired cues (Smedley et al., 2019), suggesting that reward-encoding information from the NAc is preferentially conveyed to the LHb-projecting VP DRD3$^+$ subpopulation. Inactivation of the CeA reduces cocaine self-administration (Warlow et al., 2017) and context-dependent relapse to cocaine seeking (Pelloux et al., 2018), while inhibition of glutamatergic inputs to the CeA reduces relapse after voluntary abstinence from cocaine self-administration (Venniro et al., 2017). Given that CeA neurons are predominantly GABAergic (Adams et al., 2018; Gungor et al., 2018), these findings imply that CeA inputs are preferentially inhibiting VTA-projecting VP DRD3$^+$ neurons to facilitate relapse to cocaine seeking. Enhancing this inhibition would be expected to augment cocaine seeking, which is consistent with our observation that chemogenetically inhibiting VTA-projecting VP DRD3$^+$ neurons slightly increased seeking. We note that prior findings implicating the VP to VTA projection in driving relapse to cocaine seeking (Mahler et al., 2014) used a different model of relapse in rats and did not specifically manipulate DRD3-expressing neurons, but likewise did not observe a reduction in relapse behavior with inhibition of caudal VP terminals in the VTA, suggesting that relapse model, species, cell type, and anatomical specificity may be important considerations for the VTA-projecting subpopulation.

DA-driven plasticity in the VP
In addition to anatomical input to the VP from VTA DAergic neurons (Klitenick et al., 1992) and regulation of VP DA release by drugs of abuse (Sizemore et al., 2000; Stout et al., 2016), functional evidence suggests a role for VP DA signaling in regulating local neuronal activity (Clark and Bracci, 2018; Maslowski-Cobuzzi and Napier, 1994; Mitrovic and Napier, 2002) and behavioral responses to drugs of abuse (Gong et al., 1996, 1997). Using GRAB$_{DA2m}$, we observed a robust increase in DA level in the VP in response to self-administered intravenous cocaine infusion, but unlike in the NAc latSh, spontaneous DA transients were rare, preventing us from performing a threshold-based event analysis throughout the seeking session. Our analysis of nose-poke-related GRAB$_{DA2m}$ events in the VP during seeking did not find conclusive differences between active and inactive nose pokes but warrants further investigation to understand the role of VP DA signaling during relapse, as well as in relation to DA-driven plasticity occurring during the consummatory and abstinence phases. Differentiating between DRD3-dependent plasticity occurring during the consummatory phase versus the role of elevated DRD3 expression during incubation of cocaine craving remains an open question, as does the heterogeneity of DA receptor expression in the VP. The latter point may be especially relevant in understanding why DRD3 KD restricted to LHb-projecting VP neurons was effective at reducing seeking, while DRD3 KD in the VTA projection was not.

Circuit model for role of DRD3-expressing VP neurons in cocaine seeking
In summary, our findings explain how DRD3-mediated plasticity in the VP can drive downstream changes in mesoaccumbal DA

release during relapse to cocaine seeking through a projection-defined subpopulation of neurons. We propose a circuit model (Figure S8C) detailing how reexposure to the drug-taking context elevates activity in the pallido-habenular branch of DRD3-expressing VP neurons to inhibit the LHb, which in turn disinhibits VTA DA neurons to drive release of DA in the NAc latSh. Elevated activity in this loop interlinking the NAc, VP, LHb, and midbrain may sustain an appetitive motivational state that drives cocaine seeking (Ikemoto et al., 2015). Conversely, if DRD3-mediated plasticity in the LHb-projecting branch of the VP is absent, elevated activity cannot be sustained as effectively in this loop, and drug seeking is diminished. Thus, our findings suggest that DRD3 antagonism or suppression of activity aimed at the ventral pallido-habenular branch of the reward circuitry may be an effective intervention for chronic, relapsing-remitting drug abuse.

STAR★METHODS

Detailed methods are provided in the online version of this paper and include the following:

- KEY RESOURCES TABLE
- RESOURCE AVAILABILITY
  - Lead contact
  - Materials availability
  - Data and code availability
- EXPERIMENTAL MODEL AND SUBJECT DETAILS
  - Mice
- METHOD DETAILS
  - Plasmid and virus generation
  - Surgeries
  - Behavioral procedures
  - Fiber photometry data acquisition
  - Patch clamp slice electrophysiology
  - Single-cell RT-PCR
  - Quantitative real-time PCR
  - Fluorescent *in situ* hybridization (FISH)
  - Histology and immunohistochemistry
- QUANTIFICATION AND STATISTICAL ANALYSIS
  - Fiber photometry
  - Inputs to VP DRD3$^+$ neurons
  - VP DRD3$^+$ axonal projections collateralization
  - Statistics

Neuron
Article

REFERENCES

Adams, J.M., Pei, H., Sandoval, D.A., Seeley, R.J., Chang, R.B., Liberles, S.D., and Olson, D.P. (2018). Liraglutide Modulates Appetite and Body Weight Through Glucagon-Like Peptide 1 Receptor-Expressing Glutamatergic Neurons. Diabetes 67, 1538–1548.

Adrover, M.F., Shin, J.H., and Alvarez, V.A. (2014). Glutamate and dopamine transmission from midbrain dopamine neurons share similar release properties but are differentially affected by cocaine. J. Neurosci. 34, 3183–3192.

Ahrens, A.M., Meyer, P.J., Ferguson, L.M., Robinson, T.E., and Aldridge, J.W. (2016). Neural Activity in the Ventral Pallidum Encodes Variation in the Incentive Value of a Reward Cue. J. Neurosci. 36, 7957–7970.

Akam, T., and Walton, M.E. (2019). pyPhotometry: Open source Python based hardware and software for fiber photometry data acquisition. Sci. Rep. 9, 3521.

Andreoli, M., Tessari, M., Pilla, M., Valerio, E., Hagan, J.J., and Heidbreder, C.A. (2003). Selective antagonism at dopamine D3 receptors prevents nicotine-triggered relapse to nicotine-seeking behavior. Neuropsychopharmacology 28, 1272–1280.

Araki, M., McGeer, P.L., and Kimura, H. (1988). The efferent projections of the rat lateral habenular nucleus revealed by the PHA-L anterograde tracing method. Brain Res. 441, 319–330.

Bahi, A., Boyer, F., Bussard, G., and Dreyer, J.L. (2005). Silencing dopamine D3-receptors in the nucleus accumbens shell in vivo induces changes in cocaine-induced hyperlocomotion. Eur. J. Neurosci. 21, 3415–3426.

Baik, J.H. (2013). Dopamine signaling in reward-related behaviors. Front. Neural Circuits 7, 152.

Barrot, M., Sesack, S.R., Georges, F., Pistis, M., Hong, S., and Jhou, T.C. (2012). Braking dopamine systems: a new GABA master structure for mesolimbic and nigrostriatal functions. J. Neurosci. 32, 14094–14101.

Beckstead, R.M., Wooten, G.F., and Trugman, J.M. (1988). Distribution of D1 and D2 dopamine receptors in the basal ganglia of the cat determined by quantitative autoradiography. J. Comp. Neurol. 268, 131–145.

Boileau, I., Payer, D., Houle, S., Behzadi, A., Rusjan, P.M., Tong, J., Wilkins, D., Selby, P., George, T.P., Zack, M., et al. (2012). Higher binding of the dopamine D3 receptor-preferring ligand [11C]-(+)-propyl-hexahydro-naphtho-oxazin in methamphetamine polydrug users: a positron emission tomography study. J. Neurosci. 32, 1353–1359.

Bossert, J.M., Poles, G.C., Wihbey, K.A., Koya, E., and Shaham, Y. (2007). Differential effects of blockade of dopamine D1-family receptors in nucleus ac-

cumbens core or shell on reinstatement of heroin seeking induced by contextual and discrete cues. J. Neurosci. 27, 12655–12663.

Bossert, J.M., Marchant, N.J., Calu, D.J., and Shaham, Y. (2013). The reinstatement model of drug relapse: recent neurobiological findings, emerging research topics, and translational research. Psychopharmacology (Berl.) 229, 453–476.

Brinschwitz, K., Dittgen, A., Madai, V.I., Lommel, R., Geisler, S., and Veh, R.W. (2010). Glutamatergic axons from the lateral habenula mainly terminate on GABAergic neurons of the ventral midbrain. Neuroscience 168, 463–476.

Broussard, G.J., Liang, Y., Fridman, M., Unger, E.K., Meng, G., Xiao, X., Ji, N., Petreanu, L., and Tian, L. (2018). In vivo measurement of afferent activity with axon-specific calcium imaging. Nat. Neurosci. 21, 1272–1280.

Brown, P.L., Palacorolla, H., Brady, D., Riegger, K., Elmer, G.I., and Shepard, P.D. (2017). Habenula-Induced Inhibition of Midbrain Dopamine Neurons Is Diminished by Lesions of the Rostromedial Tegmental Nucleus. J. Neurosci. 37, 217–225.

Calipari, E.S., Bagot, R.C., Purushothaman, I., Davidson, T.J., Yorgason, J.T., Peña, C.J., Walker, D.M., Pirpinias, S.T., Guise, K.G., Ramakrishnan, C., et al. (2016). In vivo imaging identifies temporal signature of D1 and D2 medium spiny neurons in cocaine reward. Proc. Natl. Acad. Sci. USA 113, 2726–2731.

Calipari, E.S., Juarez, B., Morel, C., Walker, D.M., Cahill, M.E., Ribeiro, E., Roman-Ortiz, C., Ramakrishnan, C., Deisseroth, K., Han, M.H., and Nestler, E.J. (2017). Dopaminergic dynamics underlying sex-specific cocaine reward. Nat. Commun. 8, 13877.

Cazorla, M., Shegda, M., Ramesh, B., Harrison, N.L., and Kellendonk, C. (2012). Striatal D2 receptors regulate dendritic morphology of medium spiny neurons via Kir2 channels. J. Neurosci. 32, 2398–2409.

Cetin, A., and Callaway, E.M. (2014). Optical control of retrogradely infected neurons using drug-regulated "TLoop" lentiviral vectors. J. Neurophysiol. 111, 2150–2159.

Chen, G., Kittler, J.T., Moss, S.J., and Yan, Z. (2006). Dopamine D3 receptors regulate GABAA receptor function through a phospho-dependent endocytosis mechanism in nucleus accumbens. J. Neurosci. 26, 2513–2521.

Chen, Y., Song, R., Yang, R.F., Wu, N., and Li, J. (2014). A novel dopamine D3 receptor antagonist YQA14 inhibits methamphetamine self-administration and relapse to drug-seeking behaviour in rats. Eur. J. Pharmacol. 743, 126–132.

Clark, M., and Bracci, E. (2018). Dichotomous Dopaminergic Control of Ventral Pallidum Neurons. Front. Cell. Neurosci. 12, 260.

Contreras, P.C., Quirion, R., Gehlert, D.R., Contreras, M.L., and O'Donohue, T.L. (1987). Autoradiographic distribution of non-dopaminergic binding sites labeled by [3H]haloperidol in rat brain. Neurosci. Lett. 75, 133–140.

Creed, M., Ntamati, N.R., Chandra, R., Lobo, M.K., and Lüscher, C. (2016). Convergence of Reinforcing and Anhedonic Cocaine Effects in the Ventral Pallidum. Neuron 92, 214–226.

Crombag, H.S., Grimm, J.W., and Shaham, Y. (2002). Effect of dopamine receptor antagonists on renewal of cocaine seeking by reexposure to drug-associated contextual cues. Neuropsychopharmacology 27, 1006–1015.

de Jong, J.W., Afjei, S.A., Pollak Dorocic, I., Peck, J.R., Liu, C., Kim, C.K., Tian, L., Deisseroth, K., and Lammel, S. (2019). A Neural Circuit Mechanism for Encoding Aversive Stimuli in the Mesolimbic Dopamine System. Neuron 101, 133–151.e7.

Del-Fava, F., Hasue, R.H., Ferreira, J.G., and Shammah-Lagnado, S.J. (2007). Efferent connections of the rostral linear nucleus of the ventral tegmental area in the rat. Neuroscience 145, 1059–1076.

Dong, Y., Taylor, J.R., Wolf, M.E., and Shaham, Y. (2017). Circuit and Synaptic Plasticity Mechanisms of Drug Relapse. J. Neurosci. 37, 10867–10876.

du Hoffmann, J., and Nicola, S.M. (2014). Dopamine invigorates reward seeking by promoting cue-evoked excitation in the nucleus accumbens. J. Neurosci. 34, 14349–14364.

Faget, L., Zell, V., Souter, E., McPherson, A., Ressler, R., Gutierrez-Reed, N., Yoo, J.H., Dulcis, D., and Hnasko, T.S. (2018). Opponent control of behavioral reinforcement by inhibitory and excitatory projections from the ventral pallidum. Nat. Commun. 9, 849.

CellPress
OPEN ACCESS

Neuron
Article

Farrell, M.R., Schoch, H., and Mahler, S.V. (2018). Modeling cocaine relapse in rodents: Behavioral considerations and circuit mechanisms. Prog. Neuropsychopharmacol. Biol. Psychiatry 87 (Pt A), 33–47.

Farrell, M.R., Ruiz, C.M., Castillo, E., Faget, L., Khanbijian, C., Liu, S., Schoch, H., Rojas, G., Huerta, M.Y., Hnasko, T.S., and Mahler, S.V. (2019). Ventral pallidum is essential for cocaine relapse after voluntary abstinence in rats. Neuropsychopharmacology 44, 2174–2185.

Franklin, K.B., and Paxinos, G. (2008). The Mouse Brain in Stereotaxic Coordinates, Third Edition (Academic Press), pp. 1–350.

Freeman, W.M., Lull, M.E., Patel, K.M., Brucklacher, R.M., Morgan, D., Roberts, D.C., and Vrana, K.E. (2010). Gene expression changes in the medial prefrontal cortex and nucleus accumbens following abstinence from cocaine self-administration. BMC Neurosci. 11, 29.

Fujimoto, A., Hori, Y., Nagai, Y., Kikuchi, E., Oyama, K., Suhara, T., and Minamimoto, T. (2019). Signaling Incentive and Drive in the Primate Ventral Pallidum for Motivational Control of Goal-Directed Action. J. Neurosci. 39, 1793–1804.

Galaj, E., Manuszak, M., Babic, S., Ananthan, S., and Ranaldi, R. (2015). The selective dopamine D3 receptor antagonist, SR 21502, reduces cue-induced reinstatement of heroin seeking and heroin conditioned place preference in rats. Drug Alcohol Depend. 156, 228–233.

Galaj, E., Ewing, S., and Ranaldi, R. (2018). Dopamine D1 and D3 receptor polypharmacology as a potential treatment approach for substance use disorder. Neurosci. Biobehav. Rev. 89, 13–28.

Gong, W., Neill, D., and Justice, J.B., Jr. (1996). Conditioned place preference and locomotor activation produced by injection of psychostimulants into ventral pallidum. Brain Res. 707, 64–74.

Gong, W., Neill, D., and Justice, J.B., Jr. (1997). 6-Hydroxydopamine lesion of ventral pallidum blocks acquisition of place preference conditioning to cocaine. Brain Res. 754, 103–112.

Gradinaru, V., Zhang, F., Ramakrishnan, C., Mattis, J., Prakash, R., Diester, I., Goshen, I., Thompson, K.R., and Deisseroth, K. (2010). Molecular and cellular approaches for diversifying and extending optogenetics. Cell 141, 154–165.

Gungor, N.Z., Yamamoto, R., and Pare, D. (2018). Glutamatergic and gabaergic ventral BNST neurons differ in their physiological properties and responsiveness to noradrenaline. Neuropsychopharmacology 43, 2126–2133.

Gurevich, E.V., and Joyce, J.N. (1999). Distribution of dopamine D3 receptor expressing neurons in the human forebrain: comparison with D2 receptor expressing neurons. Neuropsychopharmacology 20, 60–80.

Hamid, A.A., Pettibone, J.R., Mabrouk, O.S., Hetrick, V.L., Schmidt, R., Vander Weele, C.M., Kennedy, R.T., Aragona, B.J., and Berke, J.D. (2016). Mesolimbic dopamine signals the value of work. Nat. Neurosci. 19, 117–126.

Heinsbroek, J.A., Neuhofer, D.N., Griffin, W.C., 3rd, Siegel, G.S., Bobadilla, A.C., Kupchik, Y.M., and Kalivas, P.W. (2017). Loss of Plasticity in the D2-Accumbens Pallidal Pathway Promotes Cocaine Seeking. J. Neurosci. 37, 757–767.

Heinsbroek, J.A., Bobadilla, A.C., Dereschewitz, E., Assali, A., Chalhoub, R.M., Cowan, C.W., and Kalivas, P.W. (2020). Opposing Regulation of Cocaine Seeking by Glutamate and GABA Neurons in the Ventral Pallidum. Cell Rep. 30, 2018–2027, e2013.

Hong, S., Jhou, T.C., Smith, M., Saleem, K.S., and Hikosaka, O. (2011). Negative reward signals from the lateral habenula to dopamine neurons are mediated by rostromedial tegmental nucleus in primates. J. Neurosci. 31, 11457–11471.

Ikemoto, S., Yang, C., and Tan, A. (2015). Basal ganglia circuit loops, dopamine and motivation: A review and enquiry. Behav. Brain Res. 290, 17–31.

Ji, H., and Shepard, P.D. (2007). Lateral habenula stimulation inhibits rat midbrain dopamine neurons through a GABA(A) receptor-mediated mechanism. J. Neurosci. 27, 6923–6930.

Klitenick, M.A., Deutch, A.Y., Churchill, L., and Kalivas, P.W. (1992). Topography and functional role of dopaminergic projections from the ventral mesencephalic tegmentum to the ventral pallidum. Neuroscience 50, 371–386.

Knowland, D., Lilascharoen, V., Pacia, C.P., Shin, S., Wang, E.H., and Lim, B.K. (2017). Distinct Ventral Pallidal Neural Populations Mediate Separate Symptoms of Depression. Cell 170, 284–297.e18.

Krashes, M.J., Koda, S., Ye, C., Rogan, S.C., Adams, A.C., Cusher, D.S., Maratos-Flier, E., Roth, B.L., and Lowell, B.B. (2011). Rapid, reversible activation of AgRP neurons drives feeding behavior in mice. J. Clin. Invest. 121, 1424–1428.

Kupchik, Y.M., Scofield, M.D., Rice, K.C., Cheng, K., Roques, B.P., and Kalivas, P.W. (2014). Cocaine dysregulates opioid gating of GABA neurotransmission in the ventral pallidum. J. Neurosci. 34, 1057–1066.

Lammel, S., Lim, B.K., Ran, C., Huang, K.W., Betley, M.J., Tye, K.M., Deisseroth, K., and Malenka, R.C. (2012). Input-specific control of reward and aversion in the ventral tegmental area. Nature 491, 212–217.

Le Foll, B., Diaz, J., and Sokoloff, P. (2005). A single cocaine exposure increases BDNF and D3 receptor expression: implications for drug-conditioning. Neuroreport 16, 175–178.

Lilascharoen, V., Wang, E.H., Do, N., Pate, S.C., Tran, A.N., Yoon, C.D., Choi, J.H., Wang, X.Y., Pribiag, H., Park, Y.G., et al. (2021). Divergent pallidal pathways underlying distinct Parkinsonian behavioral deficits. Nat. Neurosci. 24, 504–515.

Lim, B.K., Huang, K.W., Grueter, B.A., Rothwell, P.E., and Malenka, R.C. (2012). Anhedonia requires MC4R-mediated synaptic adaptations in nucleus accumbens. Nature 487, 183–189.

Liu, Y., Jean-Richard-Dit-Bressel, P., Yau, J.O., Willing, A., Prasad, A.A., Power, J.M., Killcross, S., Clifford, C.W.G., and McNally, G.P. (2020). The Mesolimbic Dopamine Activity Signatures of Relapse to Alcohol-Seeking. J. Neurosci. 40, 6409–6427.

Lüscher, C., and Malenka, R.C. (2011). Drug-evoked synaptic plasticity in addiction: from molecular changes to circuit remodeling. Neuron 69, 650–663.

Mahler, S.V., Vazey, E.M., Beckley, J.T., Keistler, C.R., McGlinchey, E.M., Kaufling, J., Wilson, S.P., Deisseroth, K., Woodward, J.J., and Aston-Jones, G. (2014). Designer receptors show role for ventral pallidum input to ventral tegmental area in cocaine seeking. Nat. Neurosci. 17, 577–585.

Mahler, S.V., Brodnik, Z.D., Cox, B.M., Buchta, W.C., Bentzley, B.S., Quintanilla, J., Cope, Z.A., Lin, E.C., Riedy, M.D., Scofield, M.D., et al. (2019). Chemogenetic Manipulations of Ventral Tegmental Area Dopamine Neurons Reveal Multifaceted Roles in Cocaine Abuse. J. Neurosci. 39, 503–518.

Mansour, A., Meador-Woodruff, J.H., Bunzow, J.R., Civelli, O., Akil, H., and Watson, S.J. (1990). Localization of dopamine D2 receptor mRNA and D1 and D2 receptor binding in the rat brain and pituitary: an in situ hybridization-receptor autoradiographic analysis. J. Neurosci. 10, 2587–2600.

Maslowski-Cobuzzi, R.J., and Napier, T.C. (1994). Activation of dopaminergic neurons modulates ventral pallidal responses evoked by amygdala stimulation. Neuroscience 62, 1103–1119.

Massart, R., Barnea, R., Dikshtein, Y., Suderman, M., Meir, O., Hallett, M., Kennedy, P., Nestler, E.J., Szyf, M., and Yadid, G. (2015). Role of DNA methylation in the nucleus accumbens in incubation of cocaine craving. J. Neurosci. 35, 8042–8058.

McFarland, K., and Kalivas, P.W. (2001). The circuitry mediating cocaine-induced reinstatement of drug-seeking behavior. J. Neurosci. 21, 8655–8663.

Mengual, E., and Pickel, V.M. (2002). Ultrastructural immunocytochemical localization of the dopamine D2 receptor and tyrosine hydroxylase in the rat ventral pallidum. Synapse 43, 151–162.

Mitrovic, I., and Napier, T.C. (2002). Mu and kappa opioid agonists modulate ventral tegmental area input to the ventral pallidum. Eur. J. Neurosci. 15, 257–268.

Motulsky, H.J., and Brown, R.E. (2006). Detecting outliers when fitting data with nonlinear regression - a new method based on robust nonlinear regression and the false discovery rate. BMC Bioinformatics 7, 123.

Neisewander, J.L., Fuchs, R.A., Tran-Nguyen, L.T., Weber, S.M., Coffey, G.P., and Joyce, J.N. (2004). Increases in dopamine D3 receptor binding in rats receiving a cocaine challenge at various time points after cocaine self-

Neuron
Article

CellPress
OPEN ACCESS

administration: implications for cocaine-seeking behavior. Neuropsychopharmacology 29, 1479–1487.

Nestler, E.J., and Lüscher, C. (2019). The Molecular Basis of Drug Addiction: Linking Epigenetic to Synaptic and Circuit Mechanisms. Neuron 102, 48–59.

Osakada, F., and Callaway, E.M. (2013). Design and generation of recombinant rabies virus vectors. Nat. Protoc. 8, 1583–1601.

Ottenheimer, D.J., Bari, B.A., Sutlief, E., Fraser, K.M., Kim, T.H., Richard, J.M., Cohen, J.Y., and Janak, P.H. (2020). A quantitative reward prediction error signal in the ventral pallidum. Nat. Neurosci. 23, 1267–1276.

Papathanou, M., Dumas, S., Pettersson, H., Olson, L., and Wallén-Mackenzie, Å. (2019). Off-Target Effects in Transgenic Mice: Characterization of Dopamine Transporter (DAT)-Cre Transgenic Mouse Lines Exposes Multiple Non-Dopaminergic Neuronal Clusters Available for Selective Targeting within Limbic Neurocircuitry. eNeuro 6, ENEURO.0198-19.2019.

Pardo-Garcia, T.R., Garcia-Keller, C., Penaloza, T., Richie, C.T., Pickel, J., Hope, B.T., Harvey, B.K., Kalivas, P.W., and Heinsbroek, J.A. (2019). Ventral Pallidum Is the Primary Target for Accumbens D1 Projections Driving Cocaine Seeking. J. Neurosci. 39, 2041–2051.

Payer, D.E., Behzadi, A., Kish, S.J., Houle, S., Wilson, A.A., Rusjan, P.M., Tong, J., Selby, P., George, T.P., McCluskey, T., and Boileau, I. (2014). Heightened D3 dopamine receptor levels in cocaine dependence and contributions to the addiction behavioral phenotype: a positron emission tomography study with [11C]-+-PHNO. Neuropsychopharmacology 39, 311–318.

Pelloux, Y., Minier-Toribio, A., Hoots, J.K., Bossert, J.M., and Shaham, Y. (2018). Opposite Effects of Basolateral Amygdala Inactivation on Context-Induced Relapse to Cocaine Seeking after Extinction versus Punishment. J. Neurosci. 38, 51–59.

Petreanu, L., Mao, T., Sternson, S.M., and Svoboda, K. (2009). The subcellular organization of neocortical excitatory connections. Nature 457, 1142–1145.

Phillips, P.E., Stuber, G.D., Heien, M.L., Wightman, R.M., and Carelli, R.M. (2003). Subsecond dopamine release promotes cocaine seeking. Nature 422, 614–618.

Pickens, C.L., Airavaara, M., Theberge, F., Fanous, S., Hope, B.T., and Shaham, Y. (2011). Neurobiology of the incubation of drug craving. Trends Neurosci. 34, 411–420.

Prasad, A.A., and McNally, G.P. (2016). Ventral Pallidum Output Pathways in Context-Induced Reinstatement of Alcohol Seeking. J. Neurosci. 36, 11716–11726.

Prasad, A.A., Xie, C., Chaichim, C., Nguyen, J.H., McClusky, H.E., Killcross, S., Power, J.M., and McNally, G.P. (2020). Complementary Roles for Ventral Pallidum Cell Types and Their Projections in Relapse. J. Neurosci. 40, 880–893.

Reiner, D.J., Fredriksson, I., Lofaro, O.M., Bossert, J.M., and Shaham, Y. (2019). Relapse to opioid seeking in rat models: behavior, pharmacology and circuits. Neuropsychopharmacology 44, 465–477.

Richard, J.M., Ambroggi, F., Janak, P.H., and Fields, H.L. (2016). Ventral Pallidum Neurons Encode Incentive Value and Promote Cue-Elicited Instrumental Actions. Neuron 90, 1165–1173.

Richfield, E.K., Penney, J.B., and Young, A.B. (1989). Anatomical and affinity state comparisons between dopamine D1 and D2 receptors in the rat central nervous system. Neuroscience 30, 767–777.

Richtand, N.M. (2006). Behavioral sensitization, alternative splicing, and d3 dopamine receptor-mediated inhibitory function. Neuropsychopharmacology 31, 2368–2375.

Robinson, S.W., Jarvie, K.R., and Caron, M.G. (1994). High affinity agonist binding to the dopamine D3 receptor: chimeric receptors delineate a role for intracellular domains. Mol. Pharmacol. 46, 352–356.

Roitman, M.F., Stuber, G.D., Phillips, P.E., Wightman, R.M., and Carelli, R.M. (2004). Dopamine operates as a subsecond modulator of food seeking. J. Neurosci. 24, 1265–1271.

Root, D.H., Fabbricatore, A.T., Pawlak, A.P., Barker, D.J., Ma, S., and West, M.O. (2012). Slow phasic and tonic activity of ventral pallidal neurons during cocaine self-administration. Synapse 66, 106–127.

Root, D.H., Melendez, R.I., Zaborszky, L., and Napier, T.C. (2015). The ventral pallidum: Subregion-specific functional anatomy and roles in motivated behaviors. Prog. Neurobiol. 130, 29–70.

Salamone, J.D., and Correa, M. (2012). The mysterious motivational functions of mesolimbic dopamine. Neuron 76, 470–485.

Saunders, B.T., Yager, L.M., and Robinson, T.E. (2013). Cue-evoked cocaine "craving": role of dopamine in the accumbens core. J. Neurosci. 33, 13989–14000.

Schmittgen, T.D., and Livak, K.J. (2008). Analyzing real-time PCR data by the comparative C(T) method. Nat. Protoc. 3, 1101–1108.

Schultz, W. (2016). Dopamine reward prediction-error signalling: a two-component response. Nat. Rev. Neurosci. 17, 183–195.

Shin, S., Pribiag, H., Lilascharoen, V., Knowland, D., Wang, X.Y., and Lim, B.K. (2018). Drd3 Signaling in the Lateral Septum Mediates Early Life Stress-Induced Social Dysfunction. Neuron 97, 195–208.e6.

Sizemore, G.M., Co, C., and Smith, J.E. (2000). Ventral pallidal extracellular fluid levels of dopamine, serotonin, gamma amino butyric acid, and glutamate during cocaine self-administration in rats. Psychopharmacology (Berl.) 150, 391–398.

Smedley, E.B., DiLeo, A., and Smith, K.S. (2019). Circuit directionality for motivation: Lateral accumbens-pallidum, but not pallidum-accumbens, connections regulate motivational attraction to reward cues. Neurobiol. Learn. Mem. 162, 23–35.

Smith, K.S., Tindell, A.J., Aldridge, J.W., and Berridge, K.C. (2009). Ventral pallidum roles in reward and motivation. Behav. Brain Res. 196, 155–167.

Sokoloff, P., and Le Foll, B. (2017). The dopamine D3 receptor, a quarter century later. Eur. J. Neurosci. 45, 2–19.

Sokoloff, P., Giros, B., Martres, M.P., Bouthenet, M.L., and Schwartz, J.C. (1990). Molecular cloning and characterization of a novel dopamine receptor (D3) as a target for neuroleptics. Nature 347, 146–151.

Solecki, W., Wilczkowski, M., Pradel, K., Karwowska, K., Kielbinski, M., Drwiega, G., Zajda, K., Blasiak, T., Soltys, Z., Rajfur, Z., et al. (2020). Effects of brief inhibition of the ventral tegmental area dopamine neurons on the cocaine seeking during abstinence. Addict. Biol. 25, e12826.

Song, R., Bi, G.H., Zhang, H.Y., Yang, R.F., Gardner, E.L., Li, J., and Xi, Z.X. (2014). Blockade of D3 receptors by YQA14 inhibits cocaine's rewarding effects and relapse to drug-seeking behavior in rats. Neuropharmacology 77, 398–405.

Staley, J.K., and Mash, D.C. (1996). Adaptive increase in D3 dopamine receptors in the brain reward circuits of human cocaine fatalities. J. Neurosci. 16, 6100–6106.

Stanwood, G.D., Artymyshyn, R.P., Kung, M.P., Kung, H.F., Lucki, I., and McGonigle, P. (2000). Quantitative autoradiographic mapping of rat brain dopamine D3 binding with [(125)I]7-OH-PIPAT: evidence for the presence of D3 receptors on dopaminergic and nondopaminergic cell bodies and terminals. J. Pharmacol. Exp. Ther. 295, 1223–1231.

Stephenson-Jones, M., Bravo-Rivera, C., Ahrens, S., Furlan, A., Xiao, X., Fernandes-Henriques, C., and Li, B. (2020). Opposing Contributions of GABAergic and Glutamatergic Ventral Pallidal Neurons to Motivational Behaviors. Neuron 105, 921–933.e5.

Stout, K.A., Dunn, A.R., Lohr, K.M., Alter, S.P., Cliburn, R.A., Guillot, T.S., and Miller, G.W. (2016). Selective Enhancement of Dopamine Release in the Ventral Pallidum of Methamphetamine-Sensitized Mice. ACS Chem. Neurosci. 7, 1364–1373.

Sun, F., Zhou, J., Dai, B., Qian, T., Zeng, J., Li, X., Zhuo, Y., Zhang, Y., Wang, Y., Qian, C., et al. (2020). Next-generation GRAB sensors for monitoring dopaminergic activity in vivo. Nat. Methods 17, 1156–1166.

Swant, J., Stramiello, M., and Wagner, J.J. (2008). Postsynaptic dopamine D3 receptor modulation of evoked IPSCs via GABA(A) receptor endocytosis in rat hippocampus. Hippocampus 18, 492–502.

Tachibana, Y., and Hikosaka, O. (2012). The primate ventral pallidum encodes expected reward value and regulates motor action. Neuron 76, 826–837.

CellPress
OPEN ACCESS

Neuron
Article

Taylor, S.R., Badurek, S., Dileone, R.J., Nashmi, R., Minichiello, L., and Picciotto, M.R. (2014). GABAergic and glutamatergic efferents of the mouse ventral tegmental area. J. Comp. Neurol. *522*, 3308–3334.

Tziortzi, A.C., Searle, G.E., Tzimopoulou, S., Salinas, C., Beaver, J.D., Jenkinson, M., Laruelle, M., Rabiner, E.A., and Gunn, R.N. (2011). Imaging dopamine receptors in humans with [11C]-(+)-PHNO: dissection of D3 signal and anatomy. Neuroimage *54*, 264–277.

Venniro, M., Caprioli, D., and Shaham, Y. (2016). Animal models of drug relapse and craving: From drug priming-induced reinstatement to incubation of craving after voluntary abstinence. Prog. Brain Res. *224*, 25–52.

Venniro, M., Caprioli, D., Zhang, M., Whitaker, L.R., Zhang, S., Warren, B.L., Cifani, C., Marchant, N.J., Yizhar, O., Bossert, J.M., et al. (2017). The Anterior Insular Cortex→Central Amygdala Glutamatergic Pathway Is Critical to Relapse after Contingency Management. Neuron *96*, 414–427.e8.

Volkow, N.D., and Boyle, M. (2018). Neuroscience of Addiction: Relevance to Prevention and Treatment. Am. J. Psychiatry *175*, 729–740.

Vorel, S.R., Ashby, C.R., Jr., Paul, M., Liu, X., Hayes, R., Hagan, J.J., Middlemiss, D.N., Stemp, G., and Gardner, E.L. (2002). Dopamine D3 receptor antagonism inhibits cocaine-seeking and cocaine-enhanced brain reward in rats. J. Neurosci. *22*, 9595–9603.

Walker, D.M., Cates, H.M., Loh, Y.E., Purushothaman, I., Ramakrishnan, A., Cahill, K.M., Lardner, C.K., Godino, A., Kronman, H.G., Rabkin, J., et al. (2018). Cocaine Self-administration Alters Transcriptome-wide Responses in the Brain's Reward Circuitry. Biol. Psychiatry *84*, 867–880.

Warlow, S.M., Robinson, M.J.F., and Berridge, K.C. (2017). Optogenetic Central Amygdala Stimulation Intensifies and Narrows Motivation for Cocaine. J. Neurosci. *37*, 8330–8348.

Watabe-Uchida, M., Eshel, N., and Uchida, N. (2017). Neural Circuitry of Reward Prediction Error. Annu. Rev. Neurosci. *40*, 373–394.

Xi, Z.X., and Gardner, E.L. (2007). Pharmacological actions of NGB 2904, a selective dopamine D3 receptor antagonist, in animal models of drug addiction. CNS Drug Rev. *13*, 240–259.

Xi, Z.X., Gilbert, J.G., Pak, A.C., Ashby, C.R., Jr., Heidbreder, C.A., and Gardner, E.L. (2005). Selective dopamine D3 receptor antagonism by SB-277011A attenuates cocaine reinforcement as assessed by progressive-ratio and variable-cost-variable-payoff fixed-ratio cocaine self-administration in rats. Eur. J. Neurosci. *21*, 3427–3438.

Xi, Z.X., Li, X., Li, J., Peng, X.Q., Song, R., Gaál, J., and Gardner, E.L. (2013). Blockade of dopamine D3 receptors in the nucleus accumbens and central amygdala inhibits incubation of cocaine craving in rats. Addict. Biol. *18*, 665–677.

Yang, H., de Jong, J.W., Tak, Y., Peck, J., Bateup, H.S., and Lammel, S. (2018). Nucleus Accumbens Subnuclei Regulate Motivated Behavior via Direct Inhibition and Disinhibition of VTA Dopamine Subpopulations. Neuron *97*, 434–449.e4.

Yoo, J.H., Zell, V., Gutierrez-Reed, N., Wu, J., Ressler, R., Shenasa, M.A., Johnson, A.B., Fife, K.H., Faget, L., and Hnasko, T.S. (2016). Ventral tegmental area glutamate neurons co-release GABA and promote positive reinforcement. Nat. Commun. *7*, 13697.

You, Z.B., Bi, G.H., Galaj, E., Kumar, V., Cao, J., Gadiano, A., Rais, R., Slusher, B.S., Gardner, E.L., Xi, Z.X., and Newman, A.H. (2019). Dopamine D3R antagonist VK4-116 attenuates oxycodone self-administration and reinstatement without compromising its antinociceptive effects. Neuropsychopharmacology *44*, 1415–1424.

Neuron
Article

CellPress
OPEN ACCESS

STAR★METHODS

KEY RESOURCES TABLE

REAGENT or RESOURCE	SOURCE	IDENTIFIER
Antibodies		
anti-GFP	Thermo Fisher Scientific	A10262; RRID: AB_2534023
anti-c-Fos	Cell Signaling Technology	2250; RRID: AB_2247211
Bacterial and virus strains		
EnvA-pseudotyped, glycoprotein-deleted rabies virus; EnvA-RVΔG-eGFP	Byung Kook Lim Lab	N/A
Pseudotyped equine infectious anemia virus; RG-EIAV-DIO-Flp and RG-EIAV-Cre	Byung Kook Lim Lab	N/A
Adeno-associated virus-DJ; various	Byung Kook Lim Lab	N/A
Chemicals, peptides, and recombinant proteins		
Clozapine N-oxide	Enzo Life Sciences	BML-NS105-0025
NBQX	Tocris	0373
QX-314	Tocris	2313
Picrotoxin	Sigma	P1675
Cocaine hydrochloride	Sigma	C5776
Heparin	BD	306424
Dustless precision pellets, sugar	Bio-Serv	F05550
Tetrodotoxin	Tocris	1078
4-Aminopyridine	Sigma	275875
Red retrobeads	Lumafluor	R170
BAPTA, Tetracesium Salt, cell impermeant	Thermo Fisher Scientific	B1212
Fluoromount-G	Thermo Fisher Scientific	00-4959-52
Critical commercial assays		
Hybrid-R RNA purification kit	GeneAll	305-101
SuperScript IV First-strand cDNA synthesis kit	Thermo Fisher Scientific	18091200
TaqMan Universal Master Mix II, with UNG	Thermo Fisher Scientific	4440038
RNAscope Fluorescent Multiplex Reagent Kit	Advanced Cell Diagnostics	320850
Taqman probe: *DRD1*	Thermo Fisher Scientific	Mm02620146_s1
Taqman probe: *DRD2*	Thermo Fisher Scientific	Mm00438545_m1
Taqman probe: *DRD3*	Thermo Fisher Scientific	Mm00432887_m1
Taqman probe: *GAPDH*	Thermo Fisher Scientific	Mm99999915_g1
RNAscope probe: *DRD1a*	Advanced Cell Diagnostics	406491-C2
RNAscope probe: *DRD2*	Advanced Cell Diagnostics	406501-C3
RNAscope probe: *DRD3*	Advanced Cell Diagnostics	447721
RNAscope probe: *SLC17A6*	Advanced Cell Diagnostics	319171-C2
RNAscope probe: *SLC32A1*	Advanced Cell Diagnostics	319191-C3
RNAscope probe: *RBFOX3*	Advanced Cell Diagnostics	313311-C2
RNAscope probe: *CHAT*	Advanced Cell Diagnostics	408731-C2
RNAscope probe: *CRE recombinase*	Advanced Cell Diagnostics	312281-C2
Experimental models: cell lines		
AAV-293 cells	Agilent	240073
HEK293T cells	ATCC	CRL-3216
B7GG cells	Ed Callaway Lab; (Osakada and Callaway, 2013)	N/A
BHK-EnvA cells	Ed Callaway Lab; (Osakada and Callaway, 2013)	N/A

(*Continued on next page*)

Continued

REAGENT or RESOURCE	SOURCE	IDENTIFIER
Experimental models: organisms/strains		
Mouse: DRD3-Cre: B6.FVB(Cg)-Tg(Drd3-cre)KI196Gsat/Mmucd	GENSAT	Stock#: 036968-UCD; RRID:MMRRC_036968-UCD
Mouse: C57BL/6J	The Jackson Laboratory	JAX: 000664; RRID: IMSR_JAX:000664
Oligonucleotides		
DRD3 shRNA targeting sequence: 5′- TTCT TCTTGACTCACGTTCTT-3′	Shin et al., 2018	N/A
Single cell RT-PCR primers	See Table S1	N/A
Recombinant DNA		
pAAV-EF1α-EGFP	Shin et al., 2018	N/A
pAAV-EF1α-EmGFP-DRD3 shRNA	Shin et al., 2018	N/A
pAAV-EF1α-DRD3(T1182G)-EmGFP-DRD3 shRNA	Shin et al., 2018	N/A
pAAV-EF1α-DIO-EGFP	Shin et al., 2018	N/A
pAAV-EF1α-DIO-EmGFP-DRD3 shRNA	Shin et al., 2018	N/A
pAAV-EF1α-DIO-GCaMP6f	Shin et al., 2018	N/A
pAAV-EF1α-mCherry-DRD3 shRNA	This paper	N/A
pAAV-EF1α-DIO-GCaMP6f-DRD3 shRNA	This paper	N/A
pAAV-hSyn-GRAB$_{DA2m}$	Sun et al., 2020	N/A
pAAV-EF1α-fDIO-EGFP	Knowland et al., 2017	N/A
pAAV-EF1α-fDIO-mRuby2-TVA	Knowland et al., 2017	N/A
pAAV-EF1α-fDIO-oPBG	Knowland et al., 2017	N/A
pAAV-EF1α-DIO-mCherry	Knowland et al., 2017	N/A
pAAV-hSyn-DIO-hM4D(Gi)-mCherry	Krashes et al., 2011	Addgene plasmid # 44362
pAAV-sSyn-DIO-mRuby2-T2A-Synaptophysin-eGFP	Knowland et al., 2017	N/A
pAAV-EF1α-DIO-hChR2(H134R)-EYFP	Gift from Karl Deisseroth	Addgene plasmid # 20298
pAAV-EF1α-DIO-eNpHR3.0-EYFP	Gradinaru et al., 2010	Addgene plasmid # 26966
pAAV-hSyn-FLEX-axon-GCaMP6s-P2A-mRuby3	Broussard et al., 2018	Addgene plasmid # 112008
Software and algorithms		
Illustrator CS4	Adobe	https://www.adobe.com/
Photoshop CS4	Adobe	https://www.adobe.com/
GraphPad Prism 6	GraphPad Software	https://www.graphpad.com/
MATLAB R2015b	Mathworks	https://www.mathworks.com/products/matlab.html
FIJI (ImageJ)	NIH	https://imagej.net/Welcome
Viewer II	Biobserve	http://www.biobserve.com/behavioralresearch/products/viewer/
EthoVision XT 13	Noldus	https://www.noldus.com/
Clampfit 10.4	Molecular Devices	https://www.moleculardevices.com/products/axon-patch-clamp-system/acquisition-and-analysis-software/pclamp-software-suite
Clampex 10.4	Molecular Devices	https://www.moleculardevices.com/products/axon-patch-clamp-system/acquisition-and-analysis-software/pclamp-software-suite
MATLAB scripts for analyzing photometry data	This paper	https://github.com/VP-DRD3/Photometry-Matlab-Code

Neuron
Article

CellPress
OPEN ACCESS

Continued

REAGENT or RESOURCE	SOURCE	IDENTIFIER
MED-PC IV	Med Associates Inc	https://www.med-associates.com/tag/med-pc-iv/
MED-PC IV code for operant behaviors	This paper	https://github.com/VP-DRD3/MED-PC-Code
pyPhotometry	Akam and Walton, 2019	https://pyphotometry.readthedocs.io/en/latest/user-guide/graphical-user-interface/
OTPG8 TTL pulse generator	Doric Lenses	https://neuro.doriclenses.com/products/doric-neuroscience-studio
HCImage	Hamamatsu	https://hcimage.com/
Other		
Mouse vascular access button	Instech Laboratories	VAB62BS/22
Mouse jugular vein catheter	Access Technologies	AT-MJVC-0612A
Mono fiber-optic cannulae for fiber photometry	Doric Lenses	MFC_400/430-0.48-[length]mm_MF1.25_FLT
Dual fiber-optic cannulae for optogenetic stimulation	Doric Lenses	DFC_200/240-0.22_[length]mm_GS[spacing]_FLT
Bilateral infusions: guide cannulae	InVivo1 (P1 Technologies)	C235GS-5-[spacing]/SPC GUIDE 26GA DBL (5MM PED)
Bilateral infusions: infusion cannulae	InVivo1 (P1 Technologies)	C235IS-5/SPC INTERNAL 33GA DBL
Bilateral infusions: dummy cannulae	InVivo1 (P1 Technologies)	C235DCS-5/SPC DUMMY DBL
Infusion cannulae dust caps	InVivo1 (P1 Technologies)	303DC/1 DUST CAP

RESOURCE AVAILABILITY

Lead contact
Further information and requests for resources and reagents should be directed to and will be fulfilled by the lead contact, Byung Kook Lim (bklim@ucsd.edu).

Materials availability
DNA constructs and viruses generated by the authors will be distributed to other research investigators upon request.

Data and code availability
The data and custom code that support the findings from this study are available from the lead contact upon request.

EXPERIMENTAL MODEL AND SUBJECT DETAILS

Mice
C57BL/6J mice were obtained from The Jackson Laboratory. DRD3-Cre mice were obtained from the Gene Expression Nervous System Atlas (GENSAT, Founder line: KI196) and crossed to C57BL/6J mice for several generations prior to use. Adult male and female mice ($\sim$8-14 weeks old), housed on a 12h light/dark cycle were used for all experiments. Mice were generally housed in groups of 2-4 per cage, except for experiments involving drug infusion cannula implants, in which case they were housed individually post stereotaxic surgery. All experiments involving the use of animals were approved by the Institutional Animal Care and Use Committee (IACUC) of the University of California, San Diego.

METHOD DETAILS

Plasmid and virus generation
Adeno-associated virus (AAV) vector plasmids were generated using standard molecular cloning methods or were obtained from external sources. Origins and cloning of pAAV-EF1α-EGFP, pAAV- EF1α-EmGFP-DRD3 shRNA, pAAV-EF1α-DRD3(T1182G)-EmGFP-DRD3 shRNA (knock-down with rescue mutant), pAAV- EF1α-DIO-EGFP, pAAV-EF1α-DIO-EmGFP-DRD3 shRNA, and pAAV-EF1α-DIO-GCaMP6f were described previously (Shin et al., 2018). Construction and validation of shRNA targeting *DRD3* was described previously (Shin et al., 2018), and contained the targeting sequence 5′- TTCTTCTTGACTCACGTTCTT-3′. pAAV-EF1α-mCherry-DRD3 shRNA and pAAV-EF1α-DIO-GCaMP6f-DRD3 shRNA were generated based on pAAV-EF1α-EmGFP-DRD3 shRNA and pAAV-EF1α-DIO-EmGFP-DRD3 shRNA, respectively. pAAV-hSyn-GRAB$_{DA2m}$ was a gift from Dr. Yulong Li (Sun et al.,

2020). Origins and cloning of pAAV-EF1α-fDIO-EGFP, pAAV-EF1α-fDIO-mRuby2-TVA, pAAV-EF1α-fDIO-oPBG, pAAV-EF1α-DIO-mCherry, pAAV-hSyn-DIO-hM4D(Gi)-mCherry, pAAV-sSyn-DIO-mRuby2-T2A-Synaptophysin-eGFP, pAAV-EF1α-DIO-hChR2(H134R)-EYFP, and pAAV-EF1α-DIO-eNpHR3.0-EYFP were described previously (Knowland et al., 2017). pAAV-hSyn-DIO-axon-GCaMP6s-P2A-mRuby3 was a gift from Dr. Lin Tian (Broussard et al., 2018).

All AAV viruses used in this study were produced in-lab, as previously described (Knowland et al., 2017; Lilascharoen et al., 2021; Lim et al., 2012; Shin et al., 2018). Briefly, adenoassociated viruses (AAVs) were produced by transfection of 293 cells with three plasmids: (1) an AAV vector plasmid expressing the target construct (pAAV), (2) an AAV helper plasmid (pHELPER; Agilent), (3) and AAV-rep-cap helper plasmid (pRC-DJ, gift from M. Kay). Viral particles were isolated from cell lysates using iodixanol step-gradient ultracentrifugation and subsequently concentrated using a 100-kDa molecular mass cutoff ultrafiltration device (Millipore). Genomic titer was determined using real-time quantitative PCR and diluted in PBS to a working concentration of approximately 10^{12} viral particles/mL.

Production of EnvA-pseudotyped, glycoprotein-deleted rabies virus expressing EGFP (EnvA-RVΔG-eGFP) was described previously (Knowland et al., 2017; Lilascharoen et al., 2021; Shin et al., 2018) and based on a published protocol (Osakada and Callaway, 2013). Briefly, B7GG cells were used to generate non-pseudotyped RVΔG-eGFP, which was then pseudotyped by transducing BHK-EnVA cells.

Retrograde equine infectious anemia virus expressing Cre-dependent Flp recombinase (RG-EIAV-DIO-Flp) or Cre recombinase (RG-EIAV-Cre) was generated using a modified version of a published protocol (Cetin and Callaway, 2014), as described previously (Knowland et al., 2017; Lilascharoen et al., 2021). Briefly, HEK293T cells were transfected with three plasmids: (1) an EIAV genomic vector (pEIAV-CAG-DIO-Flp or pEIAV-CAG-Cre), (2) a helper packaging plasmid (pEV53B; a gift from John Olsen), and (3) a pseudotyping plasmid-encoding fusion protein, (FuG-B2; a gift from Kazuto Kobayashi). Viral particles were harvested from the media by centrifugation, and the resulting pellet was reconstituted with PBS and immediately stored at −80°C.

Surgeries
Stereotaxic injections
Mice were anesthetized either with a mixture of ketamine (100 mg/kg) and dexmedetomidine (0.5 mg/kg) or with isoflurane (5% for induction, 1%–2% for maintenance; Somnosuite, Kent Scientific), and then placed in a stereotaxic apparatus (David Kopf Instruments). During surgery and recovery, mice were kept on heating pads to maintain body temperature. Viral injections of 150-300 nL were delivered unilaterally or bilaterally using a Hamilton microsyringe connected to borosilicate glass pipettes, at an infusion rate of 80-100 nl/min controlled by a syringe pump (PHD Ultra, Harvard Apparatus). Pre-emptive analgesia was provided by a subcutaneous injection of buprenorphine (0.1 mg/kg) or sustained-release buprenorphine (0.5-1.0 mg/kg). Post-operative analgesia was provided by additional injections of buprenorphine (spaced 12 hr apart) or the long-lasting (72 hr) effect of sustained-release buprenorphine. For fiber photometry, optogenetic, and local chemogenetic activation experiments, optic fibers or drug-delivery cannulae were chronically implanted above the target region following viral injection, and secured to the skull with adhesive cement (C&B Metabond, Parkell). Incisions were closed with absorbable sutures (Oasis) and sterile tissue adhesive (Vetbond, 3M).

Stereotaxic coordinates were derived from Franklin and Paxino's Mouse Brain Atlas in Stereotaxic Coordinates (Franklin and Paxinos, 2008), and were as follows relative to Bregma (in mm): VP [anteroposterior (AP), +0.55; mediolateral (ML), +/−1.60; dorsoventral (DV), −5.00], NAc latSh (AP, +1.50; ML, +/− 1.60; DV, −4.40), LHb (AP, −1.00; ML, +/−0.50; DV, −2.80), VTA (AP, −3.00; ML, +/−0.60; DV, −4.70), RMTg (AP, −4.20; ML, +/−0.30; DV, −4.40). Optic fibers and drug infusion cannulae were placed ∼0.2-0.4 mm dorsal to DV coordinates. Based on histological validations, actual injection/implant sites were determined to correspond to locations approximately 0.40 mm posterior on the atlas as compared to the AP coordinates above.

For viral-mediated knock-down of *DRD3* experiments, AAV-EGFP (control), AAV-EmGFP-DRD3 shRNA (knock-down), AAV-DRD3(T1182G)-EmGFP-DRD3 shRNA (knock-down with rescue mutant)(Shin et al., 2018), AAV-mCherry-DRD3 shRNA (knock-down), AAV-DIO-EGFP (Cre-dependent control for patch clamp electrophysiology), AAV-DIO-EmGFP-DRD3 shRNA (Cre-dependent knock-down for patch clamp electrophysiology and projection-specific knock-down), AAV-DIO-GCaMP6f (control for photometry), or AAV-DIO-GCaMP6f-DRD3 shRNA (knock-down for photometry) were injected bilaterally in the VP of wild-type mice. Mice recovered for 2 weeks prior to subsequent jugular vein catheter surgery or 3 weeks prior to the start of behavioral experiments.

For identification of synaptic puncta in target regions of VP DRD3+ neurons, AAV-DIO-mRuby2-Synaptophysin-EGFP was injected unilaterally in the VP of DRD3-Cre mice; after ∼8 weeks of viral expression brains were processed for histology. We used an intersectional strategy to assess the extent to which VP DRD3+ neurons collateralize to different target regions: AAV-fDIO-EGFP was unilaterally injected in the VP, and RG-EIAV-DIO-Flp was injected in the LHb or VTA of DRD3-Cre mice; histological analyses followed after 3-4 weeks of viral expression.

For projection-defined monosynaptic rabies tracing of inputs to VP DRD3+ neurons, a 1:1 mixture of AAV-fDIO-mRuby2-TVA and AAV-fDIO-oPBG were injected in the VP, and RG-EIAV-DIO-Flp was injected into the ipsilateral LHb or VTA of DRD3-Cre mice. After 3 weeks of viral expression, the same mice were injected in the VP with EnvA-RVΔG-eGFP. After an additional 6-10 days of expression, mice were euthanized and brains were processed for histological analyses.

For calcium imaging of DRD3+ neurons in the VP, AAV-DIO-GCaMP6f or AAV-DIO-GCaMP6f-DRD3 shRNA was bilaterally injected in the VP of DRD3-Cre− mice and a photometry optic fiber (400 μm diameter, 0.48 NA, Doric Lenses) was inserted unilaterally just above the VP. For dopamine imaging in the NAc latSh and VP during self-administration experiments, AAV-GRAB_DA2m was injected

unilaterally in the NAc latSh and a 1:1 mixture of AAV-GRAB$_{DA2m}$ and AAV-mCherry-DRD3 shRNA was injected bilaterally in the VP of wild-type mice. One photometry optic fiber was inserted just above the site of virus injection in the NAc latSh while a second photometry optic fiber was inserted just above the contralateral VP. For dopamine imaging in the NAc latSh during optogenetic stimulation of VP DRD3$^+$ neuronal terminals in the LHb or VTA, AAV-GRAB$_{DA2m}$ was injected unilaterally in the NAc latSh and AAV-DIO-EYFP or AAV-DIO-ChR2-EYFP was injected bilaterally in the VP of DRD3-Cre mice. A photometry optic fiber was inserted just above the site of virus injection in the NAc latSh, and bilateral optogenetic optic fiber implants (200 μm diameter, 0.22 NA, Doric Lenses) were inserted just above the LHb or VTA. For axonal calcium imaging in the LHb and VTA, AAV-DIO-axon-GCaMP6s-P2A-mRuby3 was injected unilaterally in the VP of DRD3-Cre mice, and a photometry optic fiber was inserted above the ipsilateral LHb or VTA. Mice recovered for 2 weeks prior to subsequent jugular vein catheter surgery or 3 weeks prior to the start of behavioral experiments.

For chemogenetics experiments, AAV-DIO-hM4D(Gi)-mCherry was injected bilaterally in the VP of DRD3-Cre mice. For control of terminal activity in the LHb or VTA, bilateral drug-infusion cannulae (26 gauge, InVivo1) were inserted just above the LHb or VTA. Mice recovered for 2 weeks prior to subsequent jugular vein catheter surgery.

For optogenetic manipulations during cocaine seeking, DRD3-Cre mice were bilaterally injected with either AAV-DIO-EYFP, AAV-DIO-ChR2-EYFP or AAV-DIO-eNpHR3.0-EYFP, and dual fiber-optic cannulae (200 μm fiber diameter, 0.22 NA, Doric Lenses) were inserted just above the LHb or VTA. Mice recovered for 2 weeks prior to subsequent jugular vein catheter surgery. For ChR2-assisted circuit mapping using patch clamp electrophysiology, AAV-DIO-ChR2-EYFP was injected bilaterally in the VP of DRD3-Cre mice and *ex vivo* patch clamp recordings were performed after 3-4 weeks of viral expression.

Jugular vein catheterization

Mice were anesthetized with isoflurane (5% for induction, 1%–2% for maintenance; Somnosuite, Kent Scientific), and placed on a warming pad throughout the surgery. The right jugular vein was isolated and a silicone catheter (2 French tip size, Access Technologies) pre-filled with heparin (10 USP/mL, BD) was inserted to a depth of ∼1.2 cm toward the heart. Sutures were tied around the catheter to secure it to the vein. The other end of the catheter was attached to a mouse vascular access button (22 gauge, Instech) positioned in the interscapular area. Incisions were closed with absorbable sutures (Oasis) and sterile tissue adhesive (Vetbond, 3M). Analgesia was provided as for stereotaxic surgeries. Catheters were flushed with Heparin (100 USP/mL, BD) within a few hours of recovery from anesthesia. Mice recovered for ∼1 week prior to the start of cocaine self-administration sessions.

Behavioral procedures
Cocaine self-administration

Cocaine self-administration experiments were conducted using standard mouse operant chambers (Med-Associates) equipped with two illuminated nose pokes, a syringe pump and a vascular access button tether kit (Instech). The 'active' nose poke was paired with delivery of cocaine, whereas the 'inactive' nose poke had no consequence. Operant chambers were dark (house light off) during all sessions. Days 1-4 were conducted on a fixed-ratio 1 (FR1) schedule, and ays 5-10 were conducted on an FR3 schedule, with one session performed each day. FR sessions lasted either: (i) 2 hr for days 1-10 (for experiments presented in Figures 1D–1H and S1F–S1I), or (ii) 2 hr for day 1 and 3 hr for days 2-10 (for all other experiments involving cocaine self-administration). Prior to the start of the first session, mice were food-deprived overnight (12-16 hr) to increase exploratory behavior. Some experiments (Figures 1D–1H, S1F, and S1H) included a progressive ratio (PR) session on Day 11, with 30 min given to reach an exponentially-increasing requirement for the next infusion. Successful completion of the schedule during FR and PR sessions simultaneously resulted in: one infusion of cocaine, a 0.5 s sound cue, a 10 s illumination of the 'active' nose poke, and a 10 s time-out period during which 'active' nose pokes were recorded but did not contribute to delivery of the next infusion. Cocaine solution (Sigma-Aldrich, 0.75 mg/mL, dissolved in 0.9% saline) was delivered at a rate of ∼18 μl/sec, with each infusion delivering 1.0 mg/kg intravenously via the implanted vascular access button. One 'priming' infusion of ∼72 μL was delivered at the start of each session. For mice self-administering saline instead of cocaine, infusion volumes were equivalent. Catheters were flushed with heparin solution (100 USP/mL, BD) prior to and after the completion of each session. Catheter patency was assessed by: (i) low resistance to catheter flushing prior to the start of each session, (ii) presence of cocaine-elicited hyperlocomotor behavior at the end of each session, and (iii) infusion of sodium brevital solution (5 mg/kg) via the vascular access button to observe a rapid anesthesia response (loss of righting reflex within 5 s). Mice with poor catheter patency typically displayed a decaying nose-poking rate across days, and were removed from the study. Following the completion of all cocaine self-administration sessions, mice remained in their home cages for 2 weeks (forced abstinence). This was followed by a seeking test during which mice were re-introduced to the operant chamber, and nose pokes were recorded but had no consequence (extinction conditions). The seeking test lasted 20 min for fiber photometry experiments and 2 hr for all other experiments.

For quantitative PCR experiments, cocaine self-administration was performed as described above in the first paragraph, but the seeking test was omitted. Mice were euthanized and brain tissue was microdissected after 1 or 14 days of home-cage abstinence. Brain tissue processing and quantitative PCR were performed as described in a subsection below.

For immunostaining of c-Fos experiments, cocaine self-administration was performed as described above in the first paragraph, and mice were euthanized ∼60 min after the end of the 2hr seeking test. Brain tissue was processed as described in the histology section below.

For fiber photometry experiments, cocaine self-administration was performed as described above in the first paragraph, with some modifications. Fiber photometry measurements were made using a custom-built sCMOS camera-based set-up, described in a subsection below. Baseline photometry measurements were acquired while the (drug-naive) mouse explored the drug self-administration

operant box for 10 min on Day 0 (the day prior to the first FR1 session), with only the photometry patch cord attached to the mouse; nose poking had no consequence during this session. During days 6-10, prior to the 3 hr FR3 self-administration session, fiber photometry measurements were performed on a subset of mice, during short self-administration sessions, as follows: (i) the mouse did not receive an initial priming infusion, (ii) the first FR3 completion resulted in cue delivery only (no cocaine), (iii) the second FR3 completion resulted in cue and cocaine (1.0 mg/kg) delivery, (iv) drug was infused via a hand-held syringe to prevent the photometry patch cord and drug infusion tubing from tangling, (v) recordings proceeded for at least 2 min after the infusion, following which the mouse was returned to the home cage, (vi) visualization of the operant chamber using a near-infrared camera (Basler) facilitated these experiments. During the 20 min seeking test, only the photometry patch cord was attached to the mouse.

For experiments involving chemogenetic manipulation of the entire VP DRD3$^+$ population, cocaine self-administration was performed as described above in the first paragraph, and clozapine N-oxide (CNO) (0.1 mg/kg) was injected intraperitoneally (I.P.) ~30 min prior to the start of the seeking test (for Figures 2O–2Q) or the Day 8 FR3 session (Figures S4J–S4L). For chemogenetic control of VP DRD3$^+$ terminals in the LHb and VTA, CNO (1 mM, dissolved in ACSF, 0.2 μl/side for LHb, 0.5 μl/side for VTA) was delivered at a rate of 0.1 μl/min using a pair of Hamilton syringes connected to the chronically implanted drug infusion cannulae, ~10 min prior to the start of the 2 hr seeking test.

For patch clamp electrophysiology experiments, mice self-administered saline or cocaine for 10 days, as described above in the first paragraph. Following 12 to 16 days of home-cage abstinence, the seeking test was omitted, and mice were euthanized for *ex vivo* patch clamp electrophysiology, as described in the patch clamp slice electrophysiology section below.

For optogenetic experiments, cocaine self-administration was performed as described above in the first paragraph. Prior to the seeking test, mice were habituated to moving freely in an open field context with the optic fiber patch cord (Doric Lenses) attached to the optical fiber implant. Laser light (OEM Laser Systems) was split bilaterally through a 1x2 rotary joint (Doric Lenses). Laser power, measured with a light power meter (Thorlabs) prior to each experiment, was set to 10-15 mW bilaterally at the tip of the patch cord. During the seeking test, laser stimulation (473nm, 10 Hz, 5ms pulses for EYFP or ChR2; 593 nm, continuous for EYFP or NpHR3.0) was delivered throughout the session using an optogenetic TTL pulse generator (Doric Lenses), for alternating 10 min light ON/10 min light OFF periods, starting with a light ON period.

For projection-specific *DRD3* knock-down experiments, cocaine self-administration and the seeking test were performed exactly as described above in the first paragraph of the cocaine self-administration subsection.

Sugar pellet self-administration

Sugar pellet self-administration experiments were conducted in the same operant chambers as cocaine self-administration experiments, equipped with two illuminated nose pokes and a food pellet dispenser (Med-Associates). Mice were mildly food deprived to ~90% of free-feeding body weight throughout the experiment. The 'active' nose poke was paired with delivery of a 20 mg sugar pellet (Bio-Serv), whereas the 'inactive' nose poke had no consequence. Operant chambers were dark (house light off) during all sessions. Days 1-4 were conducted on a FR1 schedule, and days 5-10 were conducted on an FR3 schedule, with one session performed each day. FR sessions lasted 1 hr each. The PR session on Day 11 had a 30 min time-out period to reach an exponentially-increasing requirement for delivery of the next pellet. Successful completion of the schedule during FR and PR sessions simultaneously resulted in: delivery of one sugar pellet, a 0.5 s sound cue, a 10 s illumination of the 'active' nose poke, and a 10 s time-out period during which 'active' nose pokes were recorded but did not contribute to delivery of the next pellet. Following the completion of all 11 sugar self-administration sessions, mice remained in their home cages for a further two weeks. This was followed by a 1hr seeking test during which mice were reintroduced to the operant chamber and nose pokes were recorded but had no consequence (extinction conditions).

GRAB$_{DA}$ photometry with optogenetic stimulation

Mice were connected to fiber photometry and optogenetic patch cords (Doric Lenses) and placed in a clean cage with fresh bedding. Mice habituated for ~10 min to the environment prior to data acquisition. Fiber photometry measurements of GRAB$_{DA2m}$ expressed in the NAc latSh were made using an open source Python-based set-up (Akam and Walton, 2019), described in a subsection below. Optogenetic stimulation (473nm, 10 Hz, 5ms pulses, laser power 10-15 mW) was delivered for periods of 50 s, with a minimum of 60 s in between stimulation trials. Six or more stimulation trials were performed for each animal, over the course of at least 2 separate sessions.

Real-time place preference

Mice were connected to an optogenetic patch cord delivering light bilaterally via a 1x2 rotary joint (Doric Lenses). Mice were placed in a rectangular arena (L: 67.5, W:24, H: 50 cm), which had a middle section with a clear plexiglass floor (11.5 × 24 cm), and two sections on opposite sides (28 × 24 cm each) which were distinguished by wall pattern (checkered versus striped) and floor texture (smooth versus rough). Behavior was monitored using a camera (Logitech) and video tracking software (Biobserve Viewer or Noldus Ethovision XT). Mice explored the entire arena for 20 min without optical stimulation. Based on this initial habituation session, the side with lower preference was assigned as the light-paired side. Another 20 min session followed, during which presence inside the 28 × 24 cm light-paired side resulted in optogenetic stimulation (473nm, 10 Hz, 5ms pulses, laser power 10-15 mW). In some experiments, a third 20 min session followed, during which optogenetic stimulation was switched to the opposite 28 × 24 cm side. To obtain the 'light-paired side difference' value, the amount of time spent in the light-paired side during the habituation session was subtracted from the amount of time spent on the light-paired side during the stimulation session (i.e., light-paired side difference = stim. – hab.). In cases where a second stimulation session was performed, the amount of time spent in the light-paired side during the second

stimulation session was subtracted from the amount of time spent on that same side during the first stimulation session, and the average of the two light-paired side differences was calculated [i.e., light-paired side difference = (stim. 1 – hab. + stim. 2 – stim. 1)/2].

Conditioned place preference (CPP)
Experiments were conducted in a three-chambered rectangular arena (L: 67.5, W:24, H: 50 cm) with a middle chamber (11.5 × 24 cm) and two chambers on opposite sides (28 × 24 cm each) separable by two removable vertical inserts. The two chambers on each side differed in wall pattern (checkered versus striped) and floor texture (smooth versus rough). On day 1, the mouse freely explored the open arena for 20 min (habituation). On days 2-4, a morning session and an afternoon session were carried out. On day 2, the mouse was injected with saline (I.P.) in the morning session and immediately confined to one side for 15 min, while in the afternoon session, the mouse was injected with cocaine (15 mg/kg, I.P.) and immediately confined to the opposite side for 15 min. On days 3 and 4, the procedure was repeated as on day 2, with cocaine/saline and saline/cocaine administered in the morning/afternoon sessions, respectively. The cocaine-paired side was chosen randomly for each mouse. On days 5 (CPP Test 1) and 14 (CPP Test 2), the mouse freely explored the open arena again for 20 min. The amount of time spent in each chamber was tracked during the habituation and CPP Tests using a camera (Logitech) and video tracking software (Biobserve Viewer or Noldus Ethovision XT). The amount of time spent in the cocaine-paired side during the baseline session was subtracted from the amount of time spent on the same side during the CPP tests. For CPP experiments involving fiber photometry measurements, the behavioral procedures were identical, but mice were connected to a photometry patch cord on days 1, 5 and 14. Photometry data was collected and analyzed as described in a subsection below.

Open field test
Mice were placed in an open field arena (44 × 44 × 44 cm) and the total distance traveled was measured for 10 min (Biobserve). The percent time spent in the center was determined using a 20 × 20 cm zone in the center of the arena.

Fiber photometry data acquisition
Cocaine self-administration and CPP
A fiber photometry patch cord (400 μm, 0.48 NA, Doric Lenses) was coupled to the optic fiber implant using bronze sleeves (Doric Lenses) which allowed for rotational motion. Fiber photometry data was collected using a custom-built set-up with light path as follows: a 405nm/470nm/550nm LED light source (SPECTRA X, Lumencor) delivered light through an excitation filter (Thorlabs, FB410-10 and FB470-10 and M565F1), a dichroic mirror (Semrock, FF495-Di02-25 × 36) and a 20X objective (Nikon, CFI Plan Apo Lambda) connected to the optic fiber patch cord; emission light passed back through the patch cord, 20X objective, and across the dichroic mirror, on its way to an (optional) image-splitting optics unit (W-VIEW GEMINI, Hamamatsu) that separated green and red emission light. Inside the image splitter, a 560nm dichroic mirror (Chroma, T560lpxr-UF2-26 × 28 × 2 mm) separated the emission into two channels, each of which was additionally filtered by a 600-637nm (Semrock, FF01-600/37-25) or a 520-535nm emission filter (Semrock, FF01-520/35-25) and then projected onto the sCMOS camera (Orca-Flash4.0, Hamamatsu). The light source was adjusted for each mouse to generate an emission signal hovering around 20%–40% of sCMOS sensor saturation (∼40-150 μW). Images were acquired at 20 Hz using HCImage (Hamamatsu) and converted into a string of numbers (signal) using ImageJ. For self-administration experiments, HCImage acquisition and the MED-PC operant behavior program (Med-Associates) were started simultaneously; nose poke and infusion time stamps recorded by MED-PC were used to locate events in the photometry signal. GCaMP6f and $GRAB_{DA2m}$ were excited with 470 nm light. Excitation with 405 nm light (isosbestic point) for GCaMP6f and $GRAB_{DA2m}$ was performed in separate sessions; based on these recordings, contributions from motion artifacts were estimated to be much smaller than calcium- or DA release-driven transients (i.e., generally < 5% of peak transient amplitudes). Axon-GCaMP6s-P2A-mRuby3 was excited with simultaneous 470/550nm light, and image-splitting optics (W-VIEW GEMINI, Hamamatsu) separated green (GCaMP6s) and red (mRuby3) emission light into two distinct areas of the camera's field of view, allowing for separation of GCaMP6s and mRuby3 signals.

$GRAB_{DA}$ photometry with optogenetic stimulation
Mice were connected to the photometry rig using a fiber photometry patch cord and bronze sleeve, as described above for self-administration experiments. $GRAB_{DA2m}$ signals were collected using an open source, Python-based photometry rig (pyPhotometry) (Akam and Walton, 2019). Briefly, the system used 470 nm and 405 nm LEDs (Doric Lenses), a Micropython Pyboard with 2 analog and 2 digital inputs, and a photoreceiver (Doric Lenses). A graphical user interface was used to control acquisition, visualize signals and record data. Time-division multiplexed illumination allowed for interleaved acquisition of $GRAB_{DA2m}$ fluorescence evoked by 470 nm (DA-dependent) and 405 nm (DA-independent) excitation light. Optogenetic laser stimulation of ChR2 was controlled using an optogenetics TTL pulse generator (Doric Lenses) which also sent TTL pulses to one of the digital inputs on the Micropython Pyboard, allowing for precise identification of optogenetic stimulation epochs.

Patch clamp slice electrophysiology
Mice were euthanized using isofluorane inhalation and coronal brain slices (300 μm) containing either the VP, LHb or VTA were prepared using a vibratome (Leica VT1200S), in a solution containing (in mM): 110 choline chloride, 25 $NaHCO_3$, 1.25 NaH_2PO_4, 2.5 KCl, 7 $MgCl_2$, 25 glucose, 0.5 $CaCl_2$, 11.6 ascorbic acid, and 3.1 pyruvic acid, saturated with 95% O_2/5% CO_2. Slices recovered at 30°C for 20 min, and subsequently at room temperature in a solution containing (in mM): 118 NaCl, 26 $NaHCO_3$, 11 glucose, 15 HEPES, 2.5 KCl, 1.25 NaH_2PO_4, 2 pyruvic acid, 0.4 ascorbic acid, 2 $CaCl_2$, and 1 $MgCl_2$, saturated with 95% O_2/5% CO_2. Following > 1.5 hr of

recovery, slices were transferred to the electrophysiology rig's recording chamber, which was perfused with artificial cerebrospinal fluid (ACSF) containing (in mM): 119 NaCl, 26.2 NaHCO$_3$, 11 glucose, 2.5 KCl, 1 NaH$_2$PO$_4$, 2.5 CaCl$_2$, and 1.3 MgCl$_2$, saturated with 95% O$_2$/5% CO$_2$, maintained at a temperature of 30 ± 1°C and flowing at a rate of 2 mL/min. Cell soma were visualized using differential interference microscopy using 4X or 40X objectives (Olympus BX61WI). All patch clamp recordings were performed in the whole cell configuration using borosilicate glass pipettes (3-4 MΩ). Liquid junction potentials were left uncompensated. Signals were amplified and filtered (2 kHz) using an Axopatch 700B amplifier, sampled at 10 kHz using a Digidata 1550, and recorded with Clampex 10.4 (Molecular Devices). Analyses were performed offline using Clampfit 10.4 (Molecular Devices). Only cells with stable access resistance of < 25 MΩ throughout the recording period were included in the analysis.

For ChR2-assisted circuit mapping of VP DRD3$^+$ inputs to the LHb and VTA, recordings were performed following 3-4 weeks of Cre-dependent ChR2 virus expression in the VP of DRD3-Cre mice. For recordings of LHb cells projecting to the RMTg or VTA, red retrobeads (Lumafluor) were stereotaxically injected in the RMTg or VTA in the same surgery as ChR2 injections; during recordings, LHb cells containing red retrobeads were visualized using epifluorescence and selectively patched. ACSF contained 0.5 μM tetrodotoxin (TTX, Tocris) and 100 μM 4-aminopyridine (4-AP, Sigma) to isolate monosynaptic responses (Petreanu et al., 2009). Recording pipettes were filled with (in mM): 115 CsMeSO$_3$, 1.5 MgCl$_2$, 1 EGTA, 10 HEPES, 4 Mg-ATP, 0.3 Na$_3$-GTP, 10 Na-phosphocreatine, 2 QX-314, and 10 BAPTA-Cs$_4$. Excitatory to inhibitory ratio (E:I Ratio) recordings were performed in voltage clamp mode and calculated as the peak synaptic response at $V_h = -70$ mV divided by the peak synaptic response at $V_h = 0$ mV. ChR2 terminals in the LHb or VTA were activated by an LED light source (SPECTRA X, Lumencor) delivering blue light (473 nm, 5 ms pulses, ~10 mW) via the 40X objective. For each cell, 10-15 sweeps of 15 s duration were collected at each V_h for analysis, with one blue light pulse delivered at the start of each sweep. For some recordings, after obtaining E:I ratio data, ACSF containing 10 μM NBQX and/or 100 μM picrotoxin (PTX) (in addition to 0.5 μM TTX and 100 μM 4-AP) was washed onto the cells to determine whether the ChR2-evoked EPSCs or IPSCs were mediated by AMPA receptors and GABA$_A$ receptors, respectively. In all cases, EPSC or IPSC amplitude was reduced > 95% by washing on NBQX or PTX, respectively.

For studies of plasticity of VP DRD3$^+$ neurons following abstinence from saline/cocaine self-administration, recordings were performed after 12-16 days of home-cage abstinence following the last cocaine or saline self-administration session. Cells expressing Cre-dependent EGFP or Cre-dependent EGFP-DRD3 shRNA in the VP of DRD3-Cre mice were visualized using epifluorescence and selectively patched. Current clamp recordings were performed in ACSF containing 10 μM NBQX and 100 μM PTX to block synaptic transmission. For current clamp recordings, recording pipettes were filled with (in mM): 125 K-gluconate, 4 NaCl, 10 HEPES, 0.5 EGTA, 20 KCl, 4 Mg-ATP, 0.3 Na$_3$-GTP, and 10 Na-phosphocreatine. To measure firing frequency in response to current injection, cells were brought to rest at −65 mV, and +10 pA increments were applied in 500 ms steps. E:I ratio recordings were performed in voltage clamp, in plain ACSF, as for ChR2-assisted circuit mapping, but using electrical stimulation of the slice instead of blue light.

For mapping of VTA cell types receiving VP DRD3$^+$ neuronal inputs using single-cell RT-PCR, recordings were performed following 3-4 weeks of Cre-dependent ChR2 virus expression in the VP of DRD3-Cre mice. Due to the predominantly GABAergic VP DRD3$^+$ neuronal input to the VTA, we focused our analysis on cells with inhibitory ChR2-mediated responses. Recording pipettes were filled with (in mM): 125 CsCl, 8 NaCl, 0.6 EGTA, 10 HEPES, 4 Mg-ATP, 0.3 Na$_3$-GTP, 10 Na-phosphocreatine, and 2 QX-314. Recordings were performed in voltage clamp mode in the presence of 5 μM NBQX at $V_h = -70$ mV. ChR2-mediated responses were evoked with blue light stimulation, as described above. At the end of the recording, negative pressure was applied to the pipette to draw in the cytoplasmic contents of the recorded cell; the pipette tip was then crushed into the bottom of a tube containing ddH$_2$O and RNase inhibitor.

Single-cell RT-PCR
Cytoplasmic contents of each recorded cell were collected in separate tubes containing 1.5 μL ddH$_2$O and 1.0 μL RNase inhibitor. Samples were immediately stored at −80°C for subsequent batch processing. Samples were reverse transcribed using the SuperScript IV First-strand cDNA synthesis kit (Thermo Fisher Scientific). Target sequences were amplified from the cDNA by a multiplex PCR (mPCR) reaction with wide-spanning primers (~350-500 bp product size) followed by a nested PCR (nPCR) reaction (~250-300 bp product). Products were separated and visualized on 2% agarose gels. The targets amplified were: *tyrosine hydroxylase (TH)* (mPCR-F: 5'-CCGAGCCAGACTGCTGCCAC-3', mPCR-R: 5'-ACCCCCTCTAAGGAGCGCCG-3'; nPCR-F: 5'-TGGTTCACTGTGGAGTTTGGGCT-3', nPCR-R: 5'-GGGCGCTGGATACGAGAGGC −3'), *dopamine transporter (DAT)* (mPCR-F: 5'-CAGCCTGCCTGGTGCTGGTC-3', mPCR-R: 5'-AGACAGCGGGAGTGTGGCGA-3'; nPCR-F: 5'-CACAGCCCTGCTCCTGCGTG-3', nPCR-R: 5'-GCTTCTGTGCCATG TACCCCAGG-3'), *vesicular GABA transporter (VGAT)* (mPCR-F: 5'-ACTGCGACGATCTCGACTTT-3', mPCR-R: 5'-TGAGGAA CAACCCCAGGTAG-3'; nPCR-F: 5'- GCCAGGGCCTGCAGATGGAC-3', nPCR-R: 5'-CGCCGTGGAGGATGGCGTAG-3'), *vesicular glutamate transporter 2 (VGLUT2)* (mPCR-F: 5'-GGCTACTCTCATACTAGAGGG-3', mPCR-R: 5'-GCACAAATTCTTCCTTTTTCTC-3'; nPCR-F: 5'-TTGGCACGCTGTCGGGGATG-3', nPCR-R: 5'-TTCTCCTGTGAGGTAGCACCGT-3'), *glutamate decarboxylase 1 (GAD1)* (mPCR-F: 5'-CACAGGTCACCCTCGATTTT-3', mPCR-R: 5'-TCTATGCCGCTGAGTTTGTG-3'; nPCR-F: 5'-GGGCTGCGCTTGGCTT TGGA-3', nPCR-R: 5'-TGAGCAGTCCACCACCCCAGG-3'), *glutamate decarboxylase 2 (GAD2)* (mPCR-F: 5'-CAGCCTTAGGGATTG GAACA-3', mPCR-R: 5'-ACCCAGTAGTCCCCTTTGCT-3'; nPCR-F: 5'-GTTCCTTTCCTGGTGAGTGC-3', nPCR-R: 5'-TGCATCAGT CCCTCCTCTCT-3'), and *glyceraldehyde 3-phosphate dehydrogenase (GAPDH)* (mPCR-F: 5'-ACTCCACTCACGGCAAATTC-3', mPCR-R: 5'- CACATTGGGGGTAGGAACAC-3'; nPCR-F: 5'-TCTCCGCCCCTTCTGCCGAT-3', nPCR-R: 5'-CCACAGCCTTGGCAG CACCA-3'). The scRT-PCR primers listed above are also listed in Table S1.

Neuron
Article

CellPress
OPEN ACCESS

Quantitative real-time PCR

Mice were euthanized using isofluorane inhalation, and coronal brain slices (300 μm) containing the VP were prepared using a vibratome (Leica VT1200S), in standard ACSF solution containing (in mM): 119 NaCl, 26.2 NaHCO$_3$, 11 glucose, 2.5 KCl, 1 NaH$_2$PO$_4$, 2.5 CaCl$_2$, and 1.3 MgCl$_2$, saturated with 95% O$_2$/5% CO$_2$. The VP was microdissected bilaterally, immediately frozen on dry ice and then transferred to $-80°$C for subsequent batch processing. RNA was extracted using the Hybrid-R RNA purification kit (GeneAll Biotechnology). Purified RNA was reverse transcribed using the SuperScript IV First-strand cDNA synthesis kit (Thermo Fisher Scientific). Target sequences were amplified from the cDNA using the TaqMan Gene Expression Assay Kit (Thermo Fisher Scientific) and the ViiA 7 Real-Time PCR System (Thermo Fisher Scientific). Taqman probes were obtained from Thermo Fisher Scientific and were as follows: *DRD1* (Mm02620146_s1), *DRD2* (Mm00438545_m1), *DRD3* (Mm00432887_m1), *GAPDH* (Mm99999915_g1). mRNA expression level for each sample was calculated using $2^{-\Delta Ct}$, where C$_t$ was the cycle threshold for each reaction, ΔC$_t$ = C$_t$ (gene of interest) – C$_t$ (*GAPDH*) (Schmittgen and Livak, 2008). Fold change was calculated by normalizing the value of each sample to the mean of the control samples.

Fluorescent *in situ* hybridization (FISH)

Mice were euthanized using isofluorane inhalation, perfused with ice-cold ACSF, and brains were quickly extracted and placed in an isopentane bath chilled with dry ice and 70% EtOH. Coronal slices (20 μm) were sectioned using a cryostat (Leica CM3050S) and mounted on slides. Tissue processing and FISH were performed using the RNAScope Fluorescent Multiplex Assay (Advanced Cell Diagnostics), using the following probes: *Drd1a* (406491-C2), *Drd2* (406501-C3), *Drd3* (447721), *Slc17a6* (VGluT2, 319171-C2), *Slc32a1* (VGAT, 319191-C3), *NeuN* (*Rbfox3*) (313311-C2), *Chat* (408731-C2), *Cre recombinase* (312281-C2). Slides were imaged using a confocal microscope (Olympus FluoView FV1200). Several images for each anatomical area were acquired at 30X magnification, from several slices/mouse, from at least 2 mice. Quantifications were performed using the 'cell counter' function in Fiji (ImageJ). Cells were considered positive for a given marker if a cluster of $\geq$ 3 puncta surrounded the soma.

Histology and immunohistochemistry

Mice were perfused intracardially with 4% paraformaldehyde/PBS and post-fixed at 4°C overnight. For validation of GCaMP6f expression, 10 mM CaCl$_2$ was added to the perfusion solution to activate the sensor and thereby improve visualization for imaging. Coronal sections (60 μm) were sliced using a vibratome (Leica VT1000). Samples that were not immunostained were mounted directly on slides, with a DAPI counterstain. For immunohistochemistry, free-floating sections were incubated with primary antibody overnight in a PBS solution containing 10% horse serum, 0.2% bovine serum albumin, 0.5% Triton X-100, at 4°C. Sections were then washed in PBS, incubated with Alexa Fluor-conjugated secondary antibodies (1:500, Thermo Fisher Scientific) for 1hr at room temperature, washed in PBS, and then mounted on slides with DAPI counterstain medium (Fluoromount-G, Thermo Fisher Scientific). Primary antibodies were: anti-GFP to visualize GRAB$_{DA2m}$ expression (1:2000, #A10262, Thermo Fisher Scientific), and anti-c-Fos (1:5000, #2550, Cell Signaling Technology). Slides were imaged using an automated slide scanner (Olympus VS120) or a confocal microscope (Olympus FluoView FV1200). C-Fos images were quantified by applying equal thresholds to all images and using the 'analyze particles' function in ImageJ. The location of viral expression and cannula implant tracts were examined for all mice following the completion of behavioral experiments; mice with off-target expression and/or off-target implant tip location were excluded from final analyses.

QUANTIFICATION AND STATISTICAL ANALYSIS

Fiber photometry
Cocaine self-administration and CPP experiments

Signals were analyzed with Clampfit 10.4 (Molecular Devices) and MATLAB R2015b (MathWorks), and plotted with MATLAB. For analyses of GCaMP6f and GRAB$_{DA2m}$ comparing event frequency between Baseline (Day 0) and Seeking Test (Day 24) sessions, each animal performed only 1 trial for each of the two sessions, and signals from the entire duration of the sessions were analyzed as follows: (i) raw signals were adjusted to have a flat baseline using Clampfit, in a manner blind to the experimental condition; (ii) the baseline-adjusted signal was then converted to ΔF/F by dividing it by the mean of its raw signal; (iii) a value of 4 times the mean absolute deviation (4*MAD) of the Baseline (Day 0) session was used as a threshold for detecting events in both the Baseline (Day 0) and Seeking Test (Day 24) traces, with a value of 95% of 4*MAD used to re-arm event detection. The same approach was used to analyze data from CPP experiments comparing the habituation session with CPP Tests 1 and 2. For plots of the difference in total # of GCaMP6f or GRAB$_{DA2m}$ thresholded events between the Seeking and Baseline sessions (Figures S3D and S5I), the total # of thresholded events in the Baseline session was estimated by doubling the # of quantified events, to account for the fact that Baseline sessions were only 10 min long whereas Seeking Test sessions were 20 min long. For analyses of GCaMP6f event frequency change within the same session (i.e., in response to cocaine infusion), events were detected as above, and the event frequency during the 2 min after cocaine infusion was compared to the event frequency during the 2 min preceding cocaine infusion. Analyses of axon-GCaMP6s signals were performed in a similar manner to GCaMP6f analyses, but ΔF/F values were obtained by normalizing the green emission signal (axon-GCaMP6s, Ca^{2+}-dependent) to the simultaneously-acquired red emission signal (mRuby3, Ca^{2+}-independent), which served to minimize the impact of motion artifacts. Analysis of axon-GCaMP6s signals was performed by normalizing the data for each group to Day 0, in order to account for any initial differences in event frequency between VP DRD3$^+$ terminals in the LHb versus the VTA.

GRAB$_{DA2m}$ responses to cocaine infusion, as well as GCaMP6f and GRAB$_{DA2m}$ nose poke-related events during the Seeking Test (Day 24), were analyzed by focusing on signal epochs time-locked to nose pokes, using custom MATLAB scripts. Nose poke and infusion time stamps recorded by MED-PC were used to extract epochs (i.e., nose poke-related events) from the ΔF/F photometry signal. For GRAB$_{DA2m}$ responses to cocaine infusion, 1-2 trials were performed for each mouse; Area Under the Curve (AUC, 0-50sec relative to nose poke time stamp), time to peak, and half-life were determined for each trial, averaged across trials for each mouse, and then analyzed by group, with 1 data point representing each mouse. For nose poke-related events extracted from the Seeking Test, AUC (−1 to +3 s relative to nose poke time stamp) of GCaMP6f or GRAB$_{DA2m}$ signals was determined for all inactive nose pokes, but only for active nose pokes preceded by a period of > 30 s without active nose pokes, in order to avoid ambiguity in the baseline signal leading up to an active nose poke. For the GCaMP6f seeking nose poke-related analyses (Figures S3B, S3C, and S7K–S7M), AUC values were averaged for each mouse and then analyzed by group, with 1 data point representing each mouse. For the GRAB$_{DA2m}$ seeking nose poke-related analyses, AUC values were either collapsed by subject as for GCaMP6f analyses (Figures S5B, S5C, S5F, and S5G), or pooled from all subjects (Figures S5D and S5H) and statistically analyzed using analysis of covariance (ANCOVA) with subject ID as a covariate. Furthermore, for GRAB$_{DA2m}$ analyses, data was separated into the 1st 50% and the 2nd 50% of active nose pokes performed during the seeking session, in order to assess the impact of cocaine omission on DA release.

GRAB$_{DA}$ photometry with optogenetic stimulation
ΔF/F traces were obtained by normalizing the 470 nm (DA-dependent) signal to the 405 nm (DA-independent) signal. Custom MATLAB scripts were used to extract the stimulation and pre-stimulation epochs, and quantify AUC across trials and subjects. AUC was quantified instead of threshold-based event frequency because the predominant change observed was a shift in the signal baseline. Each optogenetic stimulation epoch lasted 50 s and its AUC was compared to the AUC of the 50 s epoch immediately preceding stimulation. AUC values were either collapsed by subject as for GCaMP6f analyses (Figures S7D and S7E), or pooled from all subjects (Figures 5C and 5H) and statistically analyzed using ANCOVA with subject ID as a covariate.

Inputs to VP DRD3$^+$ neurons
Sample fixation and slides were processed as described above in the histology section. Coronal sections were quantified at 120 μm intervals, approximately between AP +2.96 and −4.24 mm (Franklin and Paxinos, 2008). GFP-expressing inputs were counted using the 'cell counter' function in Fiji (ImageJ), and data were calculated as a percentage of the total number of GFP-expressing cells observed brain-wide. Inputs located around the VP injection site were not included in the total number of inputs. Anatomical regions that accounted for < 1% of total inputs were not presented in the graph.

VP DRD3$^+$ axonal projections collateralization
Sample fixation and slides were processed as described above in the histology section. Coronal sections were quantified at ∼120 μm intervals using ImageJ by applying equal thresholds to all images and measuring the thresholded area contained in a 250 × 250 pixel zone for each target. In this manner, the density of EGFP-expressing fibers could be assessed for each major VP DRD3$^+$ anatomical target. Data were presented as a percentage of the thresholded area observed in the LHb or VTA (i.e., the site of RG-EIAV-DIO-Flp injection).

Statistics
Statistical details are located in the figure legends and Table S2. Statistical analyses were performed with GraphPad Prism 6 or MATLAB R2015b. Final samples sizes were estimated using power analysis for a subset of behavioral experiments. Comparisons between two groups with normally distributed data were made using the two-tailed, unpaired Student's t test. To compare two groups with non-normal distributions or in cases where sample size was too small to determine normality, the Mann-Whitney test was used for unpaired data, and the Wilcoxon signed-rank test was used for paired data. The D'Agostino-Pearson test or the Shapiro-Wilk test were used to assess distribution normality. Analysis of covariance (ANCOVA) was performed for a subset of fiber photometry analyses in which events or trials were pooled from all subjects in order to increase statistical power; the 'separate lines' model of the 'aoctool' function in MATLAB was used, with subject ID (mouse identity) as a covariate. Differences across more than two groups were analyzed with either: (1) a one-way analysis of variance (ANOVA) for data with normal distribution and one independent variable; (2) the Kruskal-Wallis test for data with non-normal distribution and one independent variable; (3) a two-way ANOVA for data with two independent variables; or (4) a two-way repeated-measures (RM) ANOVA for data with two independent variables and multiple measurements from the same subject. ANOVAs were followed by post hoc tests with multiple comparisons correction, as indicated in the figure legends. Statistical outliers were identified using the ROUT test (Motulsky and Brown, 2006) and removed from analyses. All data are presented as mean ± standard error of the mean (SEM).